Nonlocal anisotropic elastic shell model for vibrations of double-walled carbon nanotubes under nonlinear van der Waals interaction forces

Matteo Strozzi, Valeri Smirnov, Francesco Pellicano, Margarita Kovaleva

Nonlocal anisotropic elastic shell model for vibrations of double-walled carbon nanotubes under nonlinear van der Waals interaction forces

Matteo Strozzi [a,b], Valeri V. Smirnov [c], Francesco Pellicano [b,d,*], Margarita Kovaleva [c,e]

[a] Department of Sciences and Methods for Engineering
University of Modena and Reggio Emilia
Via Amendola 2, 42122 Reggio Emilia, Italy

[b] InterMech - MO.RE. Interdepartmental Centre
Via Vivarelli 2, 41125 Modena, Italy

[c] N.N. Semenov Federal Research Center of Chemical Physics
4 Kosygin St., Moscow 119991, Russia

[d] Department of Engineering "Enzo Ferrari"
University of Modena and Reggio Emilia
Via Vivarelli 10/1, 41125 Modena, Italy

[e] Peoples Friendship University of Russia (RUDN University)
6 Miklukho-Maklaya St., Moscow 117198, Russia

N. of Pages: 51
N. of Figures: 16
N. of Tables: 7

* Corresponding Author
Prof. Francesco Pellicano, PhD
Department of Engineering "Enzo Ferrari"
University of Modena and Reggio Emilia
Via Vivarelli 10/1, 41125 Modena, Italy
Email: francesco.pellicano@unimore.it

Abstract

In this paper, a novel nonlocal anisotropic elastic shell model is developed to investigate the nonlinear vibrations of double-walled carbon nanotubes (DWCNTs) in the framework of Sanders-Koiter shell theory. Van der Waals interaction forces between the two concentric single-walled carbon nanotubes (SWCNTs) composing a DWCNT are modelled via Lennard-Jones potential and He's formulation. In the linear vibration analysis, the displacement field of each SWCNT is expanded by means of a double mixed series in terms of Chebyshev orthogonal polynomials along the longitudinal direction and harmonic functions along the circumferential direction, and Rayleigh-Ritz method is considered to get approximate natural frequencies and modal shapes. In the nonlinear vibration analysis, the three displacements of each SWCNT are re-expanded by means of the approximate eigenfunctions derived in the linear analysis, and an energy approach based on Lagrange equations is adopted to obtain a set of nonlinear ordinary differential equations of motion, which is then solved numerically. Molecular dynamics simulations are performed in order to calibrate the proper value of nonlocal parameter to be inserted in the constitutive equations of the proposed elastic continuum model. A simplified linear distribution of van der Waals interaction forces is initially adopted to analyse the nonlinear vibrations of DWCNTs, obtaining a hardening nonlinear behaviour. By considering a more realistic nonlinear distribution of van der Waals interaction forces, a stronger hardening nonlinear behaviour is found.

Keywords

Carbon nanotubes; nonlocal elasticity; anisotropic shell model; nonlinear vibrations; van der Waals interactions

1. Introduction

Carbon nanotubes (CNTs), due to their extraordinary mechanical properties, in particular very high elastic modulus and tensile strength, together with very small diameter, can reach natural frequencies of the THz order, and therefore have been considered as ideal candidates in several high sensitivity electro-mechanical devices, such as resonators, sensors and oscillators [1-4].

These relevant industrial applications have led many Researchers to focus their attention on the study of CNT vibrations, which have been investigated by means of experimental, atomistic mechanics and continuum mechanics methods.

Resonant Raman spectroscopy (RRS) represents the most common experimental technique for the study of CNT vibrations. It starts from the measurement of the diameter by means of atomic force microscopy and investigates atomic structure, chirality and natural frequencies of CNTs [5-7].

However, due to their high technological complexity, experimental techniques cannot be considered as efficient approaches for the study of CNT mechanical behaviour, especially in case of multi-walled carbon nanotubes (MWCNTs).

Molecular dynamics (MD) simulations are the most common atomistic mechanics method for the study of CNT vibrations. By considering CNT atoms as interacting point-like masses, they record CNT vibrations for a certain amount of time at fixed temperature and then compute the corresponding natural frequencies via Discrete Fourier Transform [8-10].

However, since modelling CNTs as frame-like discrete structures is computationally very expensive, then atomistic mechanics methods cannot be easily applied to the structural simulation of CNTs, in particular of MWCNTs, which incorporate a large number of carbon atoms.

Continuous elastic models are the most common continuum mechanics method for the study of CNT vibrations. In these models, actual discrete CNTs are replaced by equivalent continuous homogeneous structures, ignoring their intrinsic atomic nature and therefore reducing the number of degrees of freedom. Both beam-like [11-15] and shell-like [16-20] continuous models have been proposed.

Since theoretical models based on continuum mechanics are computationally more efficient than MD simulations and does not present the technological complexity of RRS, then they have been largely adopted for the study of CNT vibrations. In particular, the analogy between circular cylindrical shells and CNTs led to extensive application of continuous elastic shell models for CNT vibration analysis, see fundamental books of Leissa [21], Yamaki [22] and Amabili [23], where the most important thin shell theories, together with numerical and experimental results, are reported.

CNTs are frequently modelled as isotropic elastic shells [24-26]. However, there are clear indications showing that CNTs exhibit chirality-induced anisotropic behaviour that cannot be neglected [27].

Chang et al. [28] developed a molecular mechanics model, called "stick-spiral model", able to predict chirality and size-dependent elastic properties of SWCNTs. Starting from the governing equations of this model, they derived the explicit expression for longitudinal Young's modulus and Poisson's ratio, circumferential Young's modulus and Poisson's ratio, and tangential shear modulus in the case of chiral SWCNTs. In particular, they demonstrated that the classical relationship of the isotropic elastic continuum mechanics between Young's and shear moduli is no longer valid for SWCNTs.

Chang [29] derived a closed-form expression for the anisotropic surface elastic constants of SWCNTs obtained via the "stick-spiral model" of Ref. [28], and developed a molecular based anisotropic shell model able to predict the mechanical behaviour of SWCNTs. In particular, by adopting Donnell thin shell theory, he obtained explicit expressions for the coupling of axial, circumferential and torsional deformations, radial breathing mode natural frequency, and longitudinal and torsional wave speed.

Ghavanloo and Fazelzadeh [30], starting from the results of Ref. [29], developed an anisotropic elastic shell model including chirality effects to study the vibration characteristics of SWCNTs. By applying Flügge thin shell theory and complex method, they obtained natural frequencies of radial breathing, torsional, longitudinal and radial modes under different CNT diameters and chiralities. They validated their model by means of comparisons with experimental RRS and numerical MD simulation data.

Favata and Podio-Guidugli [31] developed a new orthotropic linearly elastic shell theory to study the mechanical response of MWCNTs. Starting from a modified version of the classic three-dimensional principle of virtual power, which considers a three-dimensional shell-shaped elastic body and admits thickness changes due to changes in the inter-layer separation distance of MWCNTs ("unshearability constraint" kinematic hypothesis), two-dimensional balance equations were obtained in terms of two-dimensional stress measures. The constitutive equations, derived from an orthotropic elasticity tensor and able to capture differences in chirality, were then inserted into the balance equations, in order to obtain the governing equations of motion of the new theory.

In addition to anisotropy, another relevant issue to be taken into account in the modelling of CNTs as continuous elastic shells is nonlocality. Classical continuum mechanics models assume that the stress state at a given point of a body is uniquely dependent on the strain state at the same point of the body, and they do not admit any intrinsic size dependence in their elastic constitutive equations; therefore, they are not able to identify the small-scale effect on the mechanical behaviour of CNTs. Since, at nanometre scales, the material microstructure, i.e., the lattice spacing between the individual atoms, becomes increasingly important, then the size effects are prominent, and the discrete structure of the material cannot be simply homogenised into a continuum, but the nonlocal elastic continuum model, which takes into account the scale effect, must be adopted [32].

Specifically, the nonlocal elasticity theory developed by Eringen [33-34] assumes that the stress state at a given point of a body is a function of the strain state at every point of the body, where the scale effect is inserted into the constitutive equations of the material via nonlocal parameter.

Hu et al. [35], starting from Eringen's nonlocal elasticity theory [33], developed a nonlocal elastic shell model based on Flügge thin shell theory to study transverse and torsional waves of DWCNTs. They estimated the value of the nonlocal parameter by matching CNT dispersions observed from MD simulations with numerical results obtained from nonlocal continuous elastic shell model.

Ansari et al. [36], starting from Eringen's nonlocal elasticity theory [33], developed a nonlocal shell model based on Donnell thin shell theory to analyse vibrations of DWCNTs with arbitrary boundary conditions. They calibrated the value of the nonlocal parameter by comparing natural frequencies of armchair and zigzag CNTs obtained from MD simulations with those from the nonlocal shell model. It should be underlined that many MD simulation results for DWCNTs available in literature cannot be used to calibrate the value of the nonlocal parameter within the nonlocal elastic shell models since they are referred to CNTs not respecting the hypothesis of thin shells (Kirchhoff-Love's assumptions, see Ref. [21] for more details).

As an example, Ansari et al. [37] performed MD simulations based on Tersoff-Brenner and Lennard-Jones potentials to investigate the vibration characteristics of DWCNTs under various geometries and boundary conditions, subjected to initial tensile and compressive strains. However, the results of these MD simulations cannot be used to calibrate the nonlocal parameter since the two concentric SWCNTs are not equivalent to thin cylindrical shells.

With regard to the topic analysed in the present work, a relevant paper was written by Fazelzadeh and Ghavanloo [38]. In fact, they derived for the first time a continuous elastic shell model to investigate vibrations of SWCNTs with arbitrary chirality by taking into account both nonlocal and anisotropic effects. Starting from Eringen's nonlocal elasticity theory [33], by using Flügge thin shell theory and complex method, they computed natural frequencies of SWCNTs under different values of nonlocal parameter, number of longitudinal and circumferential waves, CNT diameter and chiralities.

However, to the Authors' best knowledge, a nonlocal anisotropic elastic shell model, which combines nonlocal continuum and molecular mechanics, for the linear vibrations of DWCNTs has not yet been proposed. The first goal of the present paper is therefore to extend the nonlocal anisotropic elastic shell model for the linear vibrations of SWCNTs reported in Ref. [38] to DWCNTs. To this aim, van der Waals interactions between the two concentric SWCNTs composing a DWCNT must be properly modelled.

Ru [39] proposed a linear relationship between pressure due to van der Waals interaction forces and radial displacement for the buckling and vibration investigation of MWCNTs in which van der Waals interaction coefficient is constant, i.e., it does not depend on the radius of the individual SWCNTs. However, it is clear that this simplified formulation does not provide correct results.

In order to accurately model van der Waals interaction forces in MWCNTs, He et al. [40] proposed a linear relationship between pressure due to van der Waals interaction forces and radial displacement in which van der Waals interaction coefficient depends on the radius of the individual SWCNTs.

Based on this more refined model, natural frequencies of MWNTs were analysed by the same Authors in [41-42] for different values of SWCNT length and radius, and compared with molecular dynamics simulations for DWNTs and TWNTs, with excellent agreement.

From the papers reported above, it can be noted that the linear vibrations of CNTs have been intensely studied. Conversely, the nonlinear vibrations of CNTs have attracted much lower attention. However, the study of CNT nonlinear vibrations is very important, since nonlinear effects can strongly amplify or even modify the resonant behaviour of CNTs in their industrial applications, e.g., nano-electro-mechanical devices.

Avramov [43] investigated geometrically nonlinear vibrations of SWCNTs by means of a nonlocal elastic shell model. Sanders-Koiter shell theory was adopted to obtain the nonlinear partial differential equations of motion, which were transformed into nonlinear ordinary differential equations by means of Galerkin's method. The harmonic balance method was used to study the free nonlinear vibrations. Periodic and quasi-periodic SWCNT vibrations, owing to Naimark-Sacker bifurcation, were analysed numerically. It was found that, differently from cylindrical shells, the three displacement components (longitudinal, circumferential and radial) of the periodic and quasi-periodic SWCNT vibrations are of the same order in terms of magnitude (while, for the shells, the radial displacement component is predominant).

In addition to geometric nonlinearity, nonlinear vibrations of DWCNTs can be due also to nonlinear van der Waals interaction forces between inner and outer SWCNTs.

Fang et al. [44] performed a nonlinear vibration analysis of DWCNTs based on nonlocal elasticity theory. Ru's formulation [39] was used to model van der Waals interaction coefficient. Von Kármán geometric nonlinearity and nonlinear van der Waals interaction forces were considered. The nonlinear equations of motion were derived by adopting Euler beam theory and Hamilton principle. The effect of nonlocal parameter, aspect ratio and surrounding elastic medium on the nonlinear behaviour of DWCNTs was considered.

Xu et al. [45] studied vibrations of a DWCNT aroused by nonlinear interlayer van der Waals forces. Ru's formulation [39] was used to model van der Waals interaction coefficient. The inner and outer

SWCNTs were modelled as two individual elastic beams. Harmonic balance method was adopted to obtain the relation between amplitudes of deflection and frequencies of coaxial and noncoaxial free vibrations. The effect of aspect ratio and boundary conditions on the nonlinear behaviour of DWCNTs was investigated.

He et al. [46], starting from He's formulation [40], derived a refined nonlinear pressure distribution to describe van der Waals interactions between any two layers of a MWCNT. A continuum cylindrical shell model was used to study buckling and post-buckling of MWCNTs. By comparing the results of the linear and nonlinear van der Waals interaction force model, they found that the buckling responses before the critical buckling strain value are almost the same, while the post-buckling responses from the nonlinear model are significantly lower than those from the linear one.

Ke et al. [47] analysed nonlinear free vibrations of embedded DWCNTs based on Eringen's nonlocal elasticity theory and von Kármán geometric nonlinearity. The effect of transverse shear deformation and rotary inertia was considered in the framework of Timoshenko beam theory. Surrounding elastic medium was described via Winkler model. Ru's formulation [39] was used to model van der Waals interaction coefficient. Governing equations were derived by using Hamilton's principle. Different boundary conditions were considered. The effect of nonlocal parameter, SWCNT length and spring constant on the nonlinear vibrations of DWCNTs was investigated.

Cigeroglu and Samandari [48] studied nonlinear free vibrations of DWCNTs embedded in an elastic medium. Geometric nonlinearities due to large deflection of SWCNTs and nonlinear van der Waals interaction forces were considered. The differential quadrature method was adopted to obtain the nonlinear equations of motion. The effect of nonlinearities, boundary conditions, initial curvature and surrounding elastic medium on the nonlinear behaviour of DWCNTs was analysed.

Other relevant results on the nonlinear vibrations of CNTs and circular cylindrical shells obtained by the Authors of the present paper can be found in Refs. [49-55]. In detail, in Refs. [49-50] parametric analyses were carried out by varying aspect and thickness ratios in order to obtain a clear scenario on the influence of the geometry on the nonlinear vibrations of thin circular cylindrical shells, where the corresponding regions of softening and hardening nonlinear behaviour were derived. In addition, in Refs. [51-52] convergence analyses were performed on the nonlinear modal expansions of SWCNTs by adding suitable modes, i.e., asymmetric and axisymmetric modes, to the resonant one, in order to obtain accurate nonlinear responses with minimum computational effort. To conclude, in Refs. [53-55] nonlinear resonance interactions and dynamic stability of SWCNTs and shells were investigated.

However, in spite of some achievements in nonlinear vibration analysis of DWCNTs, to the Authors' best knowledge, there is available no attempt to tackle the topic described in the present investigation,

i.e., to study the effect of the nonlinear van der Waals interaction forces on the nonlinear vibrations of DWCNTs.

In the present paper, a novel nonlocal anisotropic elastic shell model is developed in order to study the vibrations of DWCNTs under simply supported boundary conditions. Sanders-Koiter shell theory is used to obtain the strain-displacement relationships. Lennard-Jones potential and He's formulation are used to model van der Waals interaction forces between the two concentric SWCNTs composing a DWCNT. In the linear vibration analysis, the displacement field of each SWCNT is expanded by means of a double mixed series in terms of Chebyshev orthogonal polynomials along the longitudinal direction and harmonic functions along the circumferential direction, where elastic strain, kinetic and van der Waals interaction energies are expressed in terms of the free parameters of the mixed series, and Rayleigh-Ritz method is used to obtain approximate natural frequencies and modal shapes. In the nonlinear field, the three displacements of each SWCNT are re-expanded by using the approximate eigenfunctions derived in the linear field, where elastic strain, kinetic and van der Waals interaction energies are expressed in terms of the modal coordinates, and Lagrange equations are considered to obtain a set of nonlinear ordinary differential equations of motion, which is solved numerically. In the numerical results, natural frequencies of DWCNTs are initially obtained from a local anisotropic elastic shell model. These natural frequencies are then compared with those derived from molecular dynamics simulations in order to obtain the proper value of nonlocal parameter to be inserted into the constitutive equations of the nonlocal model. Nonlinear vibrations of DWCNTs are finally obtained by adopting a nonlocal anisotropic elastic shell model and using the previously calibrated nonlocal parameter. Increasing modal initial conditions are applied on the directly excited vibration mode and corresponding amplitude-frequency curves are obtained. The nonlinear responses derived by using a linear and a nonlinear distribution of van der Waals interaction forces are compared.

2. Sanders-Koiter shell theory for DWCNTs

In the present paper, the actual discrete DWCNT of Figure 1(a) is modelled by means of a couple of concentric equivalent continuous elastic thin cylindrical shells with van der Waals interaction forces. In Figures 1(b, c) a continuous elastic thin cylindrical shell with radius R, length L and thickness h is shown; a cylindrical coordinate system (O, x, θ, z) is considered, where the origin O of the reference system is located at the centre of one end of the cylindrical shell. Three displacements are present: longitudinal $u(x, \theta, t)$, circumferential $v(x, \theta, t)$ and radial $w(x, \theta, t)$, where the radial displacement w is assumed as positive outward; (x, θ) are the longitudinal and angular coordinates of an arbitrary point on the middle surface of the shell; z is the radial coordinate along the thickness h; t is the time.

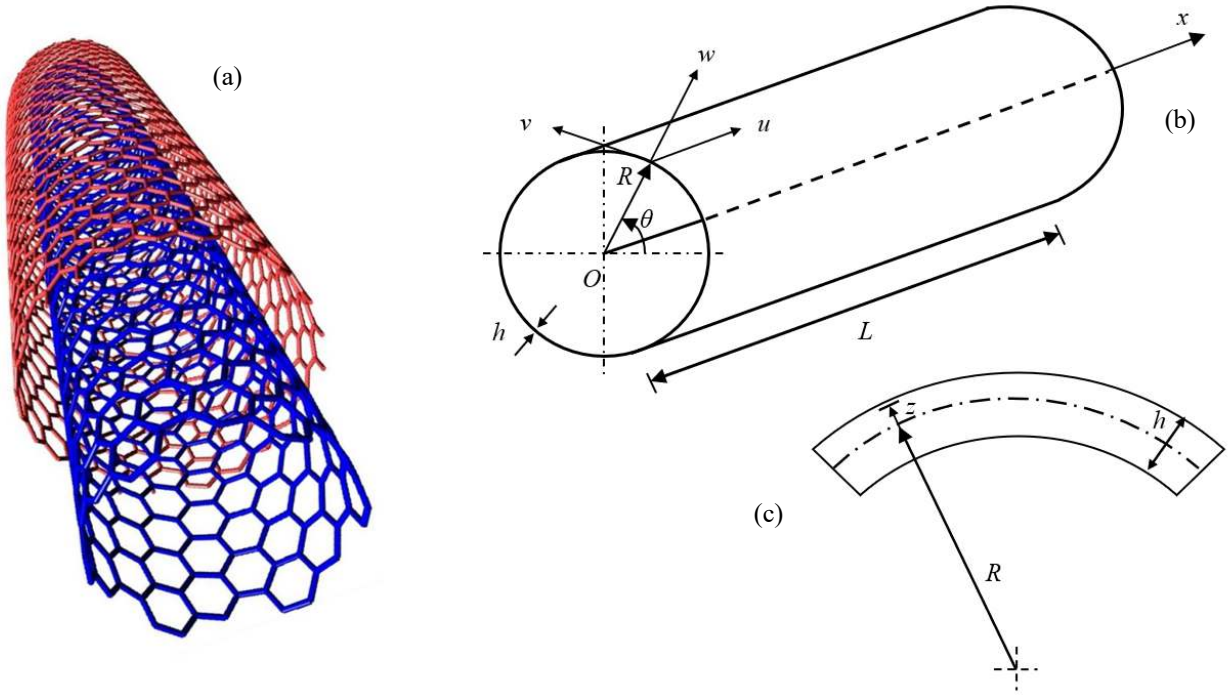

Figure 1. Continuum modelling of a DWCNT. (a) Actual discrete DWCNT. (b) Geometry of the equivalent continuous elastic thin cylindrical shell. (c) Cross-section of the surface of the equivalent continuous shell

2.1. Displacement field

The dimensionless displacement field $(\tilde{u}_i, \tilde{v}_i, \tilde{w}_i)$ of the i-th cylindrical shell is written as [20]:

$$\tilde{u}_i = \frac{u_i}{R_i} \qquad \tilde{v}_i = \frac{v_i}{R_i} \qquad \tilde{w}_i = \frac{w_i}{R_i} \qquad i = 1,2 \qquad (1)$$

where (u_i, v_i, w_i) is the dimensional displacement field and R_i is the radius of the i-th shell.

2.2. Strain-displacement relationships

In the present paper, Sanders-Koiter shell theory is used to model DWCNT dynamics. In this theory, the relationships between strains and displacements are based on "Kirchhoff-Love's assumptions", see Ref. [21] for more details.

The dimensionless middle surface strains $(\tilde{\varepsilon}_{x,0,i}, \tilde{\varepsilon}_{\theta,0,i}, \tilde{\gamma}_{x\theta,0,i})$ of the i-th cylindrical shell, taking into account both linear and nonlinear terms, are written as:

$$\tilde{\varepsilon}_{x,0,i} = \alpha_i \frac{\partial \tilde{u}_i}{\partial \eta} + \frac{1}{2}\alpha_i^2 \left(\frac{\partial \tilde{w}_i}{\partial \eta}\right)^2 + \frac{1}{8}\left(\alpha_i \frac{\partial \tilde{v}_i}{\partial \eta} - \frac{\partial \tilde{u}_i}{\partial \theta}\right)^2$$

$$\tilde{\varepsilon}_{\theta,0,i} = \frac{\partial \tilde{v}_i}{\partial \theta} + \tilde{w}_i + \frac{1}{2}\left(\frac{\partial \tilde{w}_i}{\partial \theta} - \tilde{v}_i\right)^2 + \frac{1}{8}\left(\frac{\partial \tilde{u}_i}{\partial \theta} - \alpha_i \frac{\partial \tilde{v}_i}{\partial \eta}\right)^2 \qquad i = 1,2 \qquad (2)$$

$$\tilde{\gamma}_{x\theta,0,i} = \frac{\partial \tilde{u}_i}{\partial \theta} + \alpha_i \frac{\partial \tilde{v}_i}{\partial \eta} + \alpha_i \frac{\partial \tilde{w}_i}{\partial \eta}\left(\frac{\partial \tilde{w}_i}{\partial \theta} - \tilde{v}_i\right)$$

where $\eta = x/L$ is the dimensionless longitudinal coordinate of the shell and $\alpha_i = R_i/L$.

Moreover, the dimensionless middle surface changes in curvature and torsion $(\tilde{k}_{x,i}, \tilde{k}_{\theta,i}, \tilde{k}_{x\theta,i})$ of the i-th cylindrical shell are expressed as [20]:

$$\tilde{k}_{x,i} = -\alpha_i^2 \frac{\partial^2 \tilde{w}_i}{\partial \eta^2} \qquad \tilde{k}_{\theta,i} = \frac{\partial \tilde{v}_i}{\partial \theta} - \frac{\partial^2 \tilde{w}_i}{\partial \theta^2} \qquad \tilde{k}_{x\theta,i} = -2\alpha_i \frac{\partial^2 \tilde{w}_i}{\partial \eta \partial \theta} + \frac{3}{2}\alpha_i \frac{\partial \tilde{v}_i}{\partial \eta} - \frac{1}{2}\frac{\partial \tilde{u}_i}{\partial \theta} \qquad i = 1,2 \qquad (3)$$

Finally, the dimensionless strain components $(\tilde{\varepsilon}_{x,i}, \tilde{\varepsilon}_{\theta,i}, \tilde{\gamma}_{x\theta,i})$ at a generic point of the i-th cylindrical shell are related to the dimensionless middle surface strains and changes in curvature and torsion of the i-th shell by means of the following relationships [20]:

$$\tilde{\varepsilon}_{x,i} = \tilde{\varepsilon}_{x,0,i} + \zeta_i \tilde{k}_{x,i} \qquad \tilde{\varepsilon}_{\theta,i} = \tilde{\varepsilon}_{\theta,0,i} + \zeta_i \tilde{k}_{\theta,i} \qquad \tilde{\gamma}_{x\theta,i} = \tilde{\gamma}_{x\theta,0,i} + \zeta_i \tilde{k}_{x\theta,i} \qquad i = 1,2 \qquad (4)$$

where $\zeta_i = z_i/R_i$ is the dimensionless radial coordinate of the i-th shell.

3. Nonlocal anisotropic elastic shell model for DWCNTs

In the present Section, a new nonlocal anisotropic elastic shell model for the vibrations of DWCNTs is proposed. Specifically, this model extends the nonlocal anisotropic elastic shell model for SWCNTs reported in Ref. [38] to DWCNTs.

3.1. Stress-strain relationships

By considering the plane stress hypothesis ($\sigma_z = 0$), the dimensionless stresses ($\tilde{\sigma}_{x,i}, \tilde{\sigma}_{\theta,i}, \tilde{\tau}_{x\theta,i}$) at a generic point of the i-th cylindrical shell are related to the dimensionless strains at all the other points of the i-th shell by means of the following nonlocal anisotropic elastic constitutive equations:

$$\begin{aligned}
\tilde{\sigma}_{x,i} - (e_0\tilde{a})^2\widetilde{\nabla}_i^2\tilde{\sigma}_{x,i} &= \tilde{Y}_{11,i}\tilde{\varepsilon}_{x,i} + \tilde{Y}_{12,i}\tilde{\varepsilon}_{\theta,i} + \tilde{Y}_{13,i}\tilde{\gamma}_{x\theta,i} \\
\tilde{\sigma}_{\theta,i} - (e_0\tilde{a})^2\widetilde{\nabla}_i^2\tilde{\sigma}_{\theta,i} &= \tilde{Y}_{21,i}\tilde{\varepsilon}_{x,i} + \tilde{Y}_{22,i}\tilde{\varepsilon}_{\theta,i} + \tilde{Y}_{23,i}\tilde{\gamma}_{x\theta,i} \qquad i = 1,2 \qquad (5) \\
\tilde{\tau}_{x\theta,i} - (e_0\tilde{a})^2\widetilde{\nabla}_i^2\tilde{\tau}_{x\theta,i} &= \tilde{Y}_{31,i}\tilde{\varepsilon}_{x,i} + \tilde{Y}_{32,i}\tilde{\varepsilon}_{\theta,i} + \tilde{Y}_{33,i}\tilde{\gamma}_{x\theta,i}
\end{aligned}$$

where e_0 is the unknown nonlocal parameter that must be calibrated by means of comparisons with results from molecular dynamics simulations, a is the C-C bond length and $\tilde{a} = a/R_1$ is the correlated dimensionless parameter where R_1 is the radius of the inner SWCNT, $\widetilde{\nabla}_i^2$ is the dimensionless Laplace operator expressed in polar coordinates:

$$\widetilde{\nabla}_i^2 = \alpha_i^2\frac{\partial^2}{\partial\eta^2} + \frac{\partial^2}{\partial\theta^2} \qquad i = 1,2 \qquad (6)$$

and $\tilde{Y}_{jk,i}$ are dimensionless anisotropic surface elastic constants, in the form:

$$\tilde{Y}_{jk,i} = \left(\tilde{G}_{lj,i}\tilde{G}_{lk,i} + 2\mu\widetilde{H}_{lj,i}\widetilde{H}_{lk,i}\right) \qquad j,k,l = 1,2,3 \text{ (sum over } l) \qquad i = 1,2 \qquad (7)$$

where $(\tilde{G}_{lj,i}, \tilde{G}_{lk,i}, \widetilde{H}_{lj,i}, \widetilde{H}_{lk,i})$ are dimensionless constants and μ is a dimensionless parameter [28]:

$$\mu = \frac{K_\theta}{K_\rho a^2} \qquad (8)$$

where K_ρ and K_θ are force constants associated with stretching and angular distortion of the carbon-carbon bond, respectively, and they can be obtained from quantum or empirical molecular mechanics analyses, or fitted to experimental data, see Ref. [29] for more details.

The corresponding matrices $\widetilde{\mathbf{G}}_i$ and $\widetilde{\mathbf{H}}_i$ can be calculated as follows:

$$\widetilde{\mathbf{G}}_i = \widetilde{\mathbf{B}}_i^{-1}\left(\tilde{\mathbf{I}} - \widetilde{\mathbf{D}}_i\tilde{\mathbf{F}}_i\right), \quad \widetilde{\mathbf{H}}_i = \widetilde{\mathbf{Q}}_i\tilde{\mathbf{F}}_i \qquad i = 1,2 \qquad (9)$$

where $\tilde{\mathbf{I}}$ is the identity matrix, matrix $\tilde{\mathbf{F}}_i$ is given by:

$$\tilde{\mathbf{F}}_i = \left[\tilde{\mathbf{U}}_i \tilde{\mathbf{B}}_i^{-1} \tilde{\mathbf{D}}_i - (2\mu \tilde{\mathbf{V}}_i \tilde{\mathbf{A}}_i + \tilde{\mathbf{W}}_i)\right]^{-1} \tilde{\mathbf{U}}_i \tilde{\mathbf{B}}_i^{-1} \qquad i = 1,2 \qquad (10)$$

and matrices $\left(\tilde{\mathbf{A}}_i, \tilde{\mathbf{B}}_i, \tilde{\mathbf{D}}_i, \tilde{\mathbf{U}}_i, \tilde{\mathbf{V}}_i, \tilde{\mathbf{W}}_i, \tilde{\mathbf{Q}}_i\right)$ are given by:

$$\tilde{\mathbf{A}}_i = \left\{\tilde{A}_{jk,i}\right\} = \left\{-\cos\omega_{jp,i}\cos\omega_{kp,i}\right\} \qquad j,k,p = 1,2,3 \text{ (sum over } p) \qquad i = 1,2 \qquad (11)$$

$$\tilde{\mathbf{B}}_i = \frac{1}{3\sqrt{r_i^2 + r_i s_i + s_i^2}} \begin{pmatrix} (2r_i + s_i)\cos\phi_{1,i} & -(r_i - s_i)\cos\phi_{2,i} & -(r_i + 2s_i)\cos\phi_{3,i} \\ \sqrt{3}\, s_i \sin\phi_{1,i} & -\sqrt{3}(r_i - s_i)\sin\phi_{2,i} & \sqrt{3}\, r_i \sin\phi_{3,i} \\ (2r_i + s_i)\sin\phi_{1,i} & -(r_i - s_i)\sin\phi_{2,i} & -(r_i + 2s_i)\sin\phi_{3,i} \end{pmatrix} \qquad (12)$$

$$\tilde{\mathbf{D}}_i = \frac{1}{3\sqrt{r_i^2 + r_i s_i + s_i^2}} \begin{pmatrix} -(2r_i + s_i)\sin\phi_{1,i} & (r_i - s_i)\sin\phi_{2,i} & (r_i + 2s_i)\sin\phi_{3,i} \\ \sqrt{3}\, s_i \cos\phi_{1,i} & -\sqrt{3}(r_i + s_i)\cos\phi_{2,i} & \sqrt{3}\, r_i \cos\phi_{3,i} \\ (2r_i + s_i)\cos\phi_{1,i} & -(r_i - s_i)\cos\phi_{2,i} & -(r_i + 2s_i)\cos\phi_{3,i} \end{pmatrix} \qquad (13)$$

$$\tilde{\mathbf{U}}_i = \begin{pmatrix} \sin\phi_{1,i} & \sin\phi_{2,i} & \sin\phi_{3,i} \\ \cos\phi_{1,i} & \cos\phi_{2,i} & \cos\phi_{3,i} \\ s_i\cos\phi_{1,i} & -(r_i + s_i)\cos\phi_{2,i} & r_i\cos\phi_{3,i} \end{pmatrix} \qquad (14)$$

$$\tilde{\mathbf{V}}_i = \begin{pmatrix} -\cos\phi_{1,i} & -\cos\phi_{2,i} & -\cos\phi_{3,i} \\ \sin\phi_{1,i} & \sin\phi_{2,i} & \sin\phi_{3,i} \\ 0 & 0 & 0 \end{pmatrix} \qquad (15)$$

$$\tilde{\mathbf{W}}_i = \begin{pmatrix} 0 & 0 & 0 \\ 0 & 0 & 0 \\ -s_i\sin\phi_{1,i} & (r_i + s_i)\sin\phi_{2,i} & -r_i\sin\phi_{3,i} \end{pmatrix} \qquad (16)$$

$$\tilde{\mathbf{Q}}_i = \left\{\tilde{Q}_{jk,i}\right\} = \left\{-\cos\omega_{kj,i}\right\} \qquad j,k = 1,2,3 \qquad i = 1,2 \qquad (17)$$

where:

$$\cos\omega_{jk,i} = \begin{cases} (\cos\phi_{j,i}\sin\phi_{p,i}\cos\varphi_{k,i} - \sin\phi_{j,i}\cos\phi_{p,i})/\sin\theta_{k,i} & j \neq k \neq p \\ 0 & j = k \end{cases} \qquad (18)$$

and (r_i, s_i) are the chirality indices of the i-th carbon nanotube, which define its radius [20]:

$$R_i = \frac{\sqrt{3}\,a}{2\pi}\sqrt{r_i^2 + r_i s_i + s_i^2} \tag{19}$$

The structural parameters of the i-th single-walled carbon nanotube, i.e., chiral angles $(\phi_{1,i}, \phi_{2,i}, \phi_{3,i})$ and torsion angles $(\varphi_{1,i}, \varphi_{2,i}, \varphi_{3,i})$, which can be calculated by means of the equations [30]:

$$\phi_{1,i} = \arccos\frac{2r_i + s_i}{2\sqrt{r_i^2 + r_i s_i + s_i^2}} \qquad \phi_{2,i} = \frac{4\pi}{3} + \phi_{1,i} \qquad \phi_{3,i} = \frac{2\pi}{3} + \phi_{1,i} \tag{20}$$

$$\varphi_{1,i} = \frac{\pi}{\sqrt{r_i^2 + r_i s_i + s_i^2}}\cos\phi_{1,i} \qquad \varphi_{2,i} = \frac{\pi}{\sqrt{r_i^2 + r_i s_i + s_i^2}}\cos\left(\frac{\pi}{3} + \phi_{1,i}\right)$$
$$\varphi_{3,i} = \frac{\pi}{\sqrt{r_i^2 + r_i s_i + s_i^2}}\cos\left(\frac{\pi}{3} - \phi_{1,i}\right) \tag{21}$$

and bond angles $(\theta_{1,i}, \theta_{2,i}, \theta_{3,i})$, which can be written as a function of the previous parameters in the following form [30]:

$$\cos\theta_{j,i} = \sin\phi_{k,i}\sin\phi_{p,i}\cos\varphi_{j,i} + \cos\phi_{k,i}\cos\phi_{p,i}$$
$$j, k, p = 1,2,3 \text{ (sum over } p) \qquad i = 1,2 \tag{22}$$

are illustrated in Figure 2, see Ref. [28] for more details.

It should be stressed that, in the nonlocal anisotropic elastic constitutive equations (5), the size effects are taken into account by introducing the nonlocal parameter e_0 (nonlocal model), while the chirality effects are considered by adopting the anisotropic surface elastic constants $\tilde{Y}_{jk,i}$ (anisotropic model).

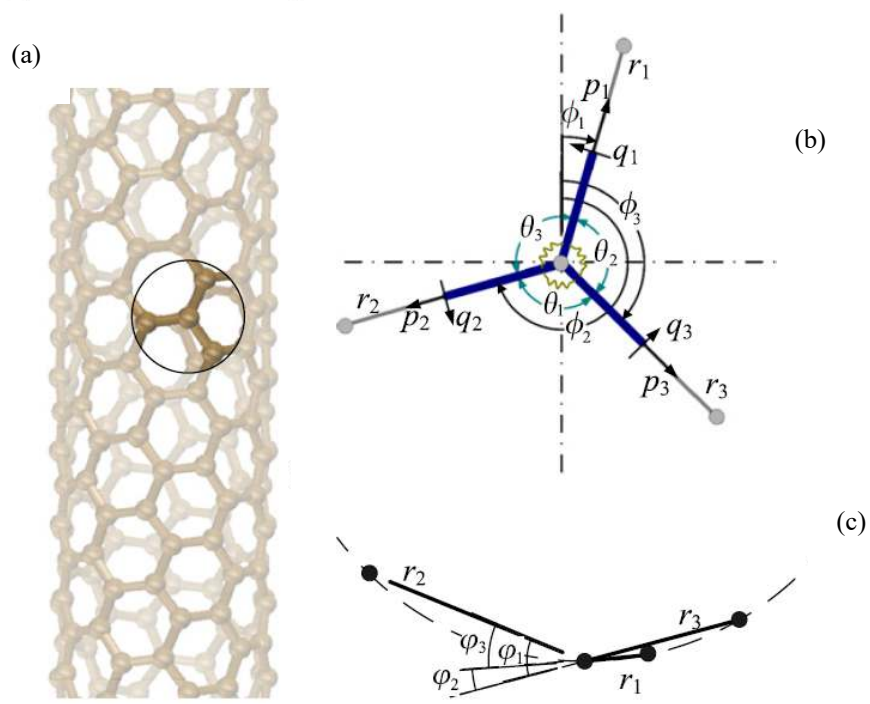

Figure 2. Schematic illustration of a (*r*, *s*) single-walled carbon nanotube. (a) Global structure with a zoom of a single representative atom; (b) side view of the local structure; (c) top view of the local structure [28]

Starting from equations (5), and assuming that carbon nanotubes satisfy the estimations $e_0 a/L \ll 1$ and $e_0 a/R \ll 1$ (i.e., accuracy is not lost by simplifying the higher order terms than the second one with respect to Laplace operator), the dimensionless stresses $(\tilde{\sigma}_{x,i}, \tilde{\sigma}_{\theta,i}, \tilde{\tau}_{x\theta,i})$ can be rewritten as:

$$\begin{aligned}
\tilde{\sigma}_{x,i} &= \tilde{Y}_{11,i}\tilde{\varepsilon}_{x,i} + \tilde{Y}_{12,i}\tilde{\varepsilon}_{\theta,i} + \tilde{Y}_{13,i}\tilde{\gamma}_{x\theta,i} + (e_0\tilde{a})^2\tilde{\nabla}_i^2\left(\tilde{Y}_{11,i}\tilde{\varepsilon}_{x,i} + \tilde{Y}_{12,i}\tilde{\varepsilon}_{\theta,i} + \tilde{Y}_{13,i}\tilde{\gamma}_{x\theta,i}\right) \\
\tilde{\sigma}_{\theta,i} &= \tilde{Y}_{21,i}\tilde{\varepsilon}_{x,i} + \tilde{Y}_{22,i}\tilde{\varepsilon}_{\theta,i} + \tilde{Y}_{23,i}\tilde{\gamma}_{x\theta,i} + (e_0\tilde{a})^2\tilde{\nabla}_i^2\left(\tilde{Y}_{21,i}\tilde{\varepsilon}_{x,i} + \tilde{Y}_{22,i}\tilde{\varepsilon}_{\theta,i} + \tilde{Y}_{23,i}\tilde{\gamma}_{x\theta,i}\right) \\
\tilde{\tau}_{x\theta,i} &= \tilde{Y}_{31,i}\tilde{\varepsilon}_{x,i} + \tilde{Y}_{32,i}\tilde{\varepsilon}_{\theta,i} + \tilde{Y}_{33,i}\tilde{\gamma}_{x\theta,i} + (e_0\tilde{a})^2\tilde{\nabla}_i^2\left(\tilde{Y}_{31,i}\tilde{\varepsilon}_{x,i} + \tilde{Y}_{32,i}\tilde{\varepsilon}_{\theta,i} + \tilde{Y}_{33,i}\tilde{\gamma}_{x\theta,i}\right)
\end{aligned} \tag{23}$$

From equations (23) it can be noted that, if it is posed $e_0 = 0$ (the nonlocal effects are removed), then the nonlocal anisotropic elastic shell model becomes a local anisotropic elastic shell model.

3.2. Force and moment resultants

Starting from the nonlocal anisotropic elastic constitutive equations (23), the correlated dimensionless force resultants per unit length of the i-th cylindrical shell $(\widetilde{N}_{x,i}, \widetilde{N}_{\theta,i}, \widetilde{N}_{x\theta,i})$ are written as a function of the corresponding dimensionless middle surface strains in the form:

$$\widetilde{N}_{x,i} = \tilde{Y}_{11,i}\tilde{\varepsilon}_{x,0,i} + \tilde{Y}_{12,i}\tilde{\varepsilon}_{\theta,0,i} + \tilde{Y}_{13,i}\tilde{\gamma}_{x\theta,0,i} + (e_0\tilde{a})^2\widetilde{\nabla}_i^2\left(\tilde{Y}_{11,i}\tilde{\varepsilon}_{x,0,i} + \tilde{Y}_{12,i}\tilde{\varepsilon}_{\theta,0,i} + \tilde{Y}_{13,i}\tilde{\gamma}_{x\theta,0,i}\right)$$

$$\widetilde{N}_{\theta,i} = \tilde{Y}_{21,i}\tilde{\varepsilon}_{x,0,i} + \tilde{Y}_{22,i}\tilde{\varepsilon}_{\theta,0,i} + \tilde{Y}_{23,i}\tilde{\gamma}_{x\theta,0,i} + (e_0\tilde{a})^2\widetilde{\nabla}_i^2\left(\tilde{Y}_{21,i}\tilde{\varepsilon}_{x,0,i} + \tilde{Y}_{22,i}\tilde{\varepsilon}_{\theta,0,i} + \tilde{Y}_{23,i}\tilde{\gamma}_{x\theta,0,i}\right) \quad (24)$$

$$\widetilde{N}_{x\theta,i} = \tilde{Y}_{31,i}\tilde{\varepsilon}_{x,0,i} + \tilde{Y}_{32,i}\tilde{\varepsilon}_{\theta,0,i} + \tilde{Y}_{33,i}\tilde{\gamma}_{x\theta,0,i} + (e_0\tilde{a})^2\widetilde{\nabla}_i^2\left(\tilde{Y}_{31,i}\tilde{\varepsilon}_{x,0,i} + \tilde{Y}_{32,i}\tilde{\varepsilon}_{\theta,0,i} + \tilde{Y}_{33,i}\tilde{\gamma}_{x\theta,0,i}\right)$$

and the correlated dimensionless moment resultants per unit length of the i-th shell ($\widetilde{M}_{x,i}, \widetilde{M}_{\theta,i}, \widetilde{M}_{x\theta,i}$) are written as a function of the corresponding dimensionless middle surface changes in curvature and torsion in the form:

$$\widetilde{M}_{x,i} = \frac{\beta_i}{12}\left(\tilde{Y}_{11,i}\tilde{k}_{x,i} + \tilde{Y}_{12,i}\tilde{k}_{\theta,i} + \tilde{Y}_{13,i}\tilde{k}_{x\theta,i} + (e_0\tilde{a})^2\widetilde{\nabla}_i^2\left(\tilde{Y}_{11,i}\tilde{k}_{x,i} + \tilde{Y}_{12,i}\tilde{k}_{\theta,i} + \tilde{Y}_{13,i}\tilde{k}_{x\theta,i}\right)\right)$$

$$\widetilde{M}_{\theta,i} = \frac{\beta_i}{12}\left(\tilde{Y}_{21,i}\tilde{k}_{x,i} + \tilde{Y}_{22,i}\tilde{k}_{\theta,i} + \tilde{Y}_{23,i}\tilde{k}_{x\theta,i} + (e_0\tilde{a})^2\widetilde{\nabla}_i^2\left(\tilde{Y}_{21,i}\tilde{k}_{x,i} + \tilde{Y}_{22,i}\tilde{k}_{\theta,i} + \tilde{Y}_{23,i}\tilde{k}_{x\theta,i}\right)\right) \quad (25)$$

$$\widetilde{M}_{x\theta,i} = \frac{\beta_i}{12}\left(\tilde{Y}_{31,i}\tilde{k}_{x,i} + \tilde{Y}_{32,i}\tilde{k}_{\theta,i} + \tilde{Y}_{33,i}\tilde{k}_{x\theta,i} + (e_0\tilde{a})^2\widetilde{\nabla}_i^2\left(\tilde{Y}_{31,i}\tilde{k}_{x,i} + \tilde{Y}_{32,i}\tilde{k}_{\theta,i} + \tilde{Y}_{33,i}\tilde{k}_{x\theta,i}\right)\right)$$

where $\beta_i = h/R_i$ is the thickness ratio of the i-th cylindrical shell.
The previous equations will be adopted into the following expressions of the boundary conditions of the i-th cylindrical shell.

3.3. Elastic strain energy

The dimensionless elastic strain energy $\widetilde{U}_i$ of the i-th cylindrical shell, which models the single-walled carbon nanotube, under plane stress hypothesis ($\sigma_z = 0$), can be expressed as follows [20]:

$$\widetilde{U}_i = \frac{1}{2}\frac{1}{\beta_i}\int_0^1\int_0^{2\pi}\int_{-\beta_i/2}^{+\beta_i/2}\left(\tilde{\sigma}_{x,i}\tilde{\varepsilon}_{x,i} + \tilde{\sigma}_{\theta,i}\tilde{\varepsilon}_{\theta,i} + \tilde{\tau}_{x\theta,i}\tilde{\gamma}_{x\theta,i}\right)d\eta d\theta d\zeta \quad (26)$$

By inserting relationships (23) and (4) into equation (26), the dimensionless elastic strain energy $\widetilde{U}_i$ of the i-th cylindrical shell, in case of homogeneous anisotropic elastic material, becomes:

$$\widetilde{U}_i = \frac{1}{2}\left(\int_0^1\int_0^{2\pi}\left(\tilde{Y}_{11,i}\tilde{\varepsilon}_{x,0,i}^2 + \tilde{Y}_{12,i}\tilde{\varepsilon}_{x,0,i}\tilde{\varepsilon}_{\theta,0,i} + \tilde{Y}_{13,i}\tilde{\varepsilon}_{x,0,i}\tilde{\gamma}_{x\theta,0,i} + \tilde{Y}_{21,i}\tilde{\varepsilon}_{x,0,i}\tilde{\varepsilon}_{\theta,0,i} +\right.\right.$$

$$\left.\left. + \tilde{Y}_{22,i}\tilde{\varepsilon}_{\theta,0,i}^2 + \tilde{Y}_{23,i}\tilde{\varepsilon}_{\theta,0,i}\tilde{\gamma}_{x\theta,0,i} + \tilde{Y}_{31,i}\tilde{\varepsilon}_{x,0,i}\tilde{\gamma}_{x\theta,0,i} + \tilde{Y}_{32,i}\tilde{\varepsilon}_{\theta,0,i}\tilde{\gamma}_{x\theta,0,i} + \tilde{Y}_{33,i}\tilde{\gamma}_{x\theta,0,i}^2\right)\right.$$

$$d\eta d\theta + \frac{\beta_i^2}{12}\int_0^1\int_0^{2\pi}\left(\tilde{Y}_{11,i}\tilde{k}_{x,i}^2 + \tilde{Y}_{12,i}\tilde{k}_{x,i}\tilde{k}_{\theta,i} + \tilde{Y}_{13,i}\tilde{k}_{x,i}\tilde{k}_{x\theta,i} + \tilde{Y}_{21,i}\tilde{k}_{x,i}\tilde{k}_{\theta,i} + \right.$$

$$+\tilde{Y}_{22,i}\tilde{k}_{\theta,i}^2 + \tilde{Y}_{23,i}\tilde{k}_{\theta,i}\tilde{k}_{x\theta,i} + \tilde{Y}_{31,i}\tilde{k}_{x,i}\tilde{k}_{x\theta,i} + \tilde{Y}_{32,i}\tilde{k}_{\theta,i}\tilde{k}_{x\theta,i} + \tilde{Y}_{33,i}\tilde{k}_{x\theta,i}^2\big)d\eta d\theta +$$

$$+(e_0\tilde{a})^2\left(\int_0^1\int_0^{2\pi}\left(\tilde{Y}_{11,i}\tilde{\varepsilon}_{x,0,i}\widetilde{\nabla}_i^2\tilde{\varepsilon}_{x,0,i} + \tilde{Y}_{12,i}\tilde{\varepsilon}_{x,0,i}\widetilde{\nabla}_i^2\tilde{\varepsilon}_{\theta,0,i} + \tilde{Y}_{13,i}\tilde{\varepsilon}_{x,0,i}\widetilde{\nabla}_i^2\tilde{\gamma}_{x\theta,0,i} + \right.\right. \quad (27)$$

$$+\tilde{Y}_{21,i}\tilde{\varepsilon}_{\theta,0,i}\widetilde{\nabla}_i^2\tilde{\varepsilon}_{x,0,i} + \tilde{Y}_{22,i}\tilde{\varepsilon}_{\theta,0,i}\widetilde{\nabla}_i^2\tilde{\varepsilon}_{\theta,0,i} + \tilde{Y}_{23,i}\tilde{\varepsilon}_{\theta,0,i}\widetilde{\nabla}_i^2\tilde{\gamma}_{x\theta,0,i} + \tilde{Y}_{31,i}\tilde{\gamma}_{x\theta,0,i}\widetilde{\nabla}_i^2\tilde{\varepsilon}_{x,0,i} +$$

$$+\tilde{Y}_{32,i}\tilde{\gamma}_{x\theta,0,i}\widetilde{\nabla}_i^2\tilde{\varepsilon}_{\theta,0,i} + \tilde{Y}_{33,i}\tilde{\gamma}_{x\theta,0,i}\widetilde{\nabla}_i^2\tilde{\gamma}_{x\theta,0,i}\big)d\eta d\theta + \frac{\beta_i^2}{12}\int_0^1\int_0^{2\pi}\left(\tilde{Y}_{11,i}\tilde{k}_{x,i}\widetilde{\nabla}_i^2\tilde{k}_{x,i} + \right.$$

$$+\tilde{Y}_{12,i}\tilde{k}_{x,i}\widetilde{\nabla}_i^2\tilde{k}_{\theta,i} + \tilde{Y}_{13,i}\tilde{k}_{x,i}\widetilde{\nabla}_i^2\tilde{k}_{x\theta,i} + \tilde{Y}_{21,i}\tilde{k}_{\theta,i}\widetilde{\nabla}_i^2\tilde{k}_{x,i} + \tilde{Y}_{22,i}\tilde{k}_{\theta,i}\widetilde{\nabla}_i^2\tilde{k}_{\theta,i} +$$

$$\left.\left.+\tilde{Y}_{23,i}\tilde{k}_{\theta,i}\widetilde{\nabla}_i^2\tilde{k}_{x\theta,i} + \tilde{Y}_{31,i}\tilde{k}_{x\theta,i}\widetilde{\nabla}_i^2\tilde{k}_{x,i} + \tilde{Y}_{32,i}\tilde{k}_{x\theta,i}\widetilde{\nabla}_i^2\tilde{k}_{\theta,i} + \tilde{Y}_{33,i}\tilde{k}_{x\theta,i}\widetilde{\nabla}_i^2\tilde{k}_{x\theta,i}\big)d\eta d\theta\right)\right)$$

In equation (27), the first two terms on the right-hand side are associated with a local model: the first term, which is related to the middle surface strains of the shell, represents the local stretching energy, while the second one, which is related to the middle surface changes in curvature and torsion of the shell, represents the local bending energy [23].

Moreover, in equation (27), the third and the fourth terms on the right-hand side are connected with a nonlocal model: the third term, which is related to the middle surface strains of the shell, represents the nonlocal stretching energy, while the fourth one, which is related to the middle surface changes in curvature and torsion of the shell, represents the nonlocal bending energy.

The dimensionless elastic strain energy of a DWCNT, given by two concentric SWCNTs, is [20]:

$$\widetilde{U} = \sum_{i=1}^{2}\delta_i\widetilde{U}_i \quad (28)$$

where $\delta_i = R_i/R_1$ and R_1 is the radius of the inner SWCNT.

3.4. Kinetic energy

The dimensional time variable t is made dimensionless by adopting a reference frequency ω_0, which denotes the lowest extensional circular frequency of an anisotropic ring under plane strain hypothesis, expressed in the form [26]:

$$\omega_0 = \sqrt{\frac{Y}{\rho h R_1^2}} \tag{29}$$

where:

$$Y = \frac{2K_\rho}{3\sqrt{3}} \tag{30}$$

is a reference dimensional surface elastic constant, ρ and h are mass density and thickness of the two layers of the DWCNT, respectively, and $\tau = \omega_0 t$ is the dimensionless time variable.
The dimensionless velocity field of the i-th cylindrical shell $(\tilde{u}_i', \tilde{v}_i', \tilde{w}_i')$ is written in the form [20]:

$$\tilde{u}_i' = \frac{d\tilde{u}_i}{d\tau} = \frac{\dot{u}_i}{R_i\omega_0} \qquad \tilde{v}_i' = \frac{d\tilde{v}_i}{d\tau} = \frac{\dot{v}_i}{R_i\omega_0} \qquad \tilde{w}_i' = \frac{d\tilde{w}_i}{d\tau} = \frac{\dot{w}_i}{R_i\omega_0} \qquad i = 1,2 \tag{31}$$

where $(\dot{u}_i, \dot{v}_i, \dot{w}_i)$ is the corresponding dimensional velocity field.
The dimensionless kinetic energy of the i-th cylindrical shell, which models the single-walled carbon nanotube, by neglecting the rotary inertia effect, is given by [20]:

$$\tilde{T}_i = \frac{1}{2}\delta_i^2 \int_0^1 \int_0^{2\pi} (\tilde{u}_i'^2 + \tilde{v}_i'^2 + \tilde{w}_i'^2) d\eta d\theta \qquad i = 1,2 \tag{32}$$

The dimensionless kinetic energy of a DWCNT, given by two concentric SWCNTs, is [20]:

$$\tilde{T} = \sum_{i=1}^{2} \delta_i \tilde{T}_i \tag{33}$$

3.4. Nonlinear van der Waals interaction energy

Van der Waals interaction forces between the two layers (i, j) of a DWCNT can be modelled starting from the dimensionless Lennard-Jones pair potential [41]:

$$\tilde{V}_{LJ}(\tilde{a}) = 4\tilde{\varepsilon}\left(\left(\frac{\tilde{\sigma}}{\tilde{a}}\right)^{12} - \left(\frac{\tilde{\sigma}}{\tilde{a}}\right)^{6}\right) \tag{34}$$

where ε is the C-C potential depth and $\tilde{\varepsilon} = \varepsilon/YR_1^2$ is the correlated dimensionless parameter, σ is the C-C equilibrium separation distance and $\tilde{\sigma} = \sigma/R_1$ is the correlated dimensionless parameter.

The dimensionless van der Waals interaction force is found by deriving the dimensionless Lennard-Jones pair potential (34) with respect to the C-C atom distance [41]:

$$\tilde{F}(\tilde{a}) = -\frac{d\tilde{V}_{LJ}(\tilde{a})}{d\tilde{a}} = \frac{24\tilde{\varepsilon}}{\tilde{\sigma}}\left(2\left(\frac{\tilde{\sigma}}{\tilde{a}}\right)^{13} - \left(\frac{\tilde{\sigma}}{\tilde{a}}\right)^{7}\right) \tag{35}$$

In order to properly investigate the effect of van der Waals interactions on the mechanical behaviour of DWCNTs, we have to expand the dimensionless van der Waals interaction force (35) not only to the first-order term (i.e. linear analysis), therefore neglecting the change in distance between the two layers of the DWCNT due to van der Waals interactions, but at least up to the third-order term (i.e. cubic nonlinearity) [46]:

$$\tilde{F}(\tilde{a}) = \tilde{F}(\tilde{a}_0) + \frac{d\tilde{F}(\tilde{a}_0)}{d\tilde{a}_0}(\tilde{a} - \tilde{a}_0) + \frac{1}{6}\frac{d^3\tilde{F}(\tilde{a}_0)}{d\tilde{a}_0^3}(\tilde{a} - \tilde{a}_0)^3 \tag{36}$$

where $\tilde{a}_0$ is the dimensionless initial C-C atom distance of the two layers prior to bucking.
It should be observed that in expansion (36) the second-order term (i.e. quadratic nonlinearity) is not present, this is because van der Waals interaction force (35) is an odd function of $\tilde{a}$. Moreover, if in expansion (36) also the third-order term is eliminated, then the linear van der Waals interaction force is obtained.
By substituting equation (35) into expansion (36) it is derived [46]:

$$\begin{aligned}\tilde{F}(\tilde{a}) = {} & \frac{24\tilde{\varepsilon}}{\tilde{\sigma}}\left(2\left(\frac{\tilde{\sigma}}{\tilde{a}_0}\right)^{13} - \left(\frac{\tilde{\sigma}}{\tilde{a}_0}\right)^{7}\right) - \frac{24\tilde{\varepsilon}}{\tilde{\sigma}^2}\left(26\left(\frac{\tilde{\sigma}}{\tilde{a}_0}\right)^{14} - 77\left(\frac{\tilde{\sigma}}{\tilde{a}_0}\right)^{8}\right)\cdot \\ & \cdot(\tilde{a} - \tilde{a}_0) - \frac{24\tilde{\varepsilon}}{\tilde{\sigma}^4}\left(910\left(\frac{\tilde{\sigma}}{\tilde{a}_0}\right)^{16} - 84\left(\frac{\tilde{\sigma}}{\tilde{a}_0}\right)^{10}\right)\cdot(\tilde{a} - \tilde{a}_0)^3\end{aligned} \tag{37}$$

At the equilibrium position prior to buckling, the initial van der Waals interaction force $\tilde{F}(\tilde{a}_0)$ is very small and it can be neglected. By integrating equation (37) over the entire DWCNT, it is obtained the dimensionless pressure $\tilde{p}_i$ exerted on the i-th SWCNT due to van der Waals interactions between the two layers (i, j), expressed as a function of the dimensionless radial displacements $(\widetilde{w}_i, \widetilde{w}_j)$ [46]:

$$\tilde{p}_i(\eta, \theta) = \tilde{c}_{ij}\left(\delta_i\widetilde{w}_i - \delta_j\widetilde{w}_j\right) + \tilde{e}_{ij}(\delta_i\widetilde{w}_i - \delta_j\widetilde{w}_j)^3 \qquad i, j = 1,2 \qquad i \neq j \tag{38}$$

where $(\tilde{c}_{ij}, \tilde{e}_{ij})$ are dimensionless van der Waals interaction coefficients between the layers (i, j).

These coefficients can be expressed by adopting He's formulation in the following form [46]:

$$\tilde{c}_{ij} = -\left(\frac{1001\pi\tilde{\varepsilon}\tilde{\sigma}^{12}}{3\tilde{a}^4}\tilde{E}_{ij}^{13} - \frac{1120\pi\tilde{\varepsilon}\tilde{\sigma}^{6}}{9\tilde{a}^4}\tilde{E}_{ij}^{7}\right)\delta_j$$
$$\tilde{e}_{ij} = -\left(\frac{65065\pi\tilde{\varepsilon}\tilde{\sigma}^{12}}{6\tilde{a}^4}\tilde{E}_{ij}^{15} - \frac{3920\pi\tilde{\varepsilon}\tilde{\sigma}^{6}}{3\tilde{a}^4}\tilde{E}_{ij}^{9}\right)\delta_j \qquad i,j = 1,2 \qquad i \neq j \qquad (39)$$

The dimensionless elliptical integral $\tilde{E}_{ij}^{m}$ of the interaction coefficients (39) is written as [42]:

$$\tilde{E}_{ij}^{m} = (\delta_j + \delta_i)^{-m}\int_0^{\pi/2}\frac{d\theta}{(1-\tilde{k}_{ij}\cos^2\theta)^{m/2}} \qquad i,j = 1,2 \qquad i \neq j \qquad m = 7,9,13,15 \qquad (40)$$

where the dimensionless geometric coefficient $\tilde{k}_{ij}$ of the integrals (40) is expressed as [42]:

$$\tilde{k}_{ij} = \frac{4\delta_j\delta_i}{(\delta_j + \delta_i)^2} \qquad i,j = 1,2 \qquad i \neq j \qquad (41)$$

The dimensionless van der Waals interaction energy of the *i*-th cylindrical shell, which models the single-walled carbon nanotube, is expressed as follows [20]:

$$\tilde{V}_i = -\frac{1}{2}\delta_i\int_0^1\int_0^{2\pi}\tilde{p}_i(\eta,\theta)\tilde{w}_i d\eta d\theta \qquad i = 1,2 \qquad (42)$$

and the dimensionless van der Waals interaction energy of a DWCNT is [20]:

$$\tilde{V} = \sum_{i=1}^{2}\delta_i\tilde{V}_i \qquad (43)$$

4. Vibration modelling of DWCNTs

In order to perform the vibration analysis of DWCNTs, a two-step energy based procedure is adopted: (i) in the linear field, the displacement field of each SWCNT is expanded by means of a double mixed series, the elastic strain, kinetic and van der Waals interaction energies of the DWCNT are expressed in terms of free parameters of the series and Rayleigh-Ritz method is used to get approximate natural frequencies and modal shapes; (ii) in the nonlinear field, the three displacements of each SWCNT are re-expanded by considering the approximate eigenfunctions derived in the linear analysis, the elastic strain, kinetic and van der Waals interaction energies of the DWCNT are expressed in terms of modal

coordinates and Lagrange equations are adopted to obtain a system of nonlinear ordinary differential equations of motion, which is then solved numerically.

4.1. Linear vibration analysis

In the linear vibration analysis, only the linear terms within the expressions of the elastic strain energy (27) and van der Waals interaction energy (42) are considered.

A modal vibration, i.e. a synchronous motion, of a DWCNT, composed by two concentric SWCNTs, which are modelled as thin cylindrical shells, can be formally written as [20]:

$$\tilde{u}_i(\eta,\theta,\tau) = \widetilde{U}_i(\eta,\theta)\tilde{f}_i(\tau) \qquad \tilde{v}_i(\eta,\theta,\tau) = \widetilde{V}_i(\eta,\theta)\tilde{f}_i(\tau) \qquad \widetilde{w}_i(\eta,\theta,\tau) = \widetilde{W}_i(\eta,\theta)\tilde{f}_i(\tau) \qquad i = 1,2 \qquad (44)$$

where $(\widetilde{U}_i, \widetilde{V}_i, \widetilde{W}_i)$ are the three dimensionless components of the modal shape of the i-th cylindrical shell and $\tilde{f}_i(\tau)$ is the corresponding dimensionless time law, which is supposed to be the same for the three dimensionless displacements $(\tilde{u}_i, \tilde{v}_i, \widetilde{w}_i)$ (modal vibration hypothesis).

The modal shape components $(\widetilde{U}_i, \widetilde{V}_i, \widetilde{W}_i)$ are expanded by means of a double mixed series in terms of m-th degree Chebyshev orthogonal polynomials $T_m^*(\eta)$ along the longitudinal direction η and harmonic functions $(\cos n\theta\,, \sin n\theta)$ along the circumferential direction θ, in the form [26]:

$$\widetilde{U}_i(\eta,\theta) = \sum_{m=0}^{M_u}\sum_{n=0}^{N} \widetilde{U}_{i,m,n} T_m^*(\eta)\cos n\theta \qquad \widetilde{V}_i(\eta,\theta) = \sum_{m=0}^{M_v}\sum_{n=0}^{N} \widetilde{V}_{i,m,n} T_m^*(\eta)\sin n\theta \qquad \widetilde{W}_i(\eta,\theta) = \sum_{m=0}^{M_w}\sum_{n=0}^{N} \widetilde{W}_{i,m,n} T_m^*(\eta)\cos n\theta \qquad i = 1,2 \qquad (45)$$

where $T_m^* = T_m(2\eta - 1)$, m denotes the number of longitudinal half-waves, n represents the number of circumferential waves and $(\widetilde{U}_{i,m,n}, \widetilde{V}_{i,m,n}, \widetilde{W}_{i,m,n})$ are unknown coefficients, which can be obtained by imposing the boundary conditions.

4.2. Boundary conditions

In this paper, simply supported DWCNTs are analysed. The corresponding boundary conditions are expressed in the form [26]:

$$\tilde{v}_i = 0 \qquad \widetilde{w}_i = 0 \qquad \widetilde{N}_{x,i} = 0 \qquad \widetilde{M}_{x,i} = 0 \qquad \eta = 0,1 \qquad i = 1,2 \qquad (46)$$

Starting from conditions (46), taking into consideration equations (24,25) for the dimensionless force and moment resultants, equations (44) for the dimensionless displacements, and expansions (45) for the corresponding modal shape components, the following relationships are derived [26]:

$$\begin{aligned}
\tilde{V}_i(\eta,\theta) &= \sum_{m=0}^{M_v}\sum_{n=0}^{N} \tilde{V}_{i,m,n} T_m^*(\eta)\sin n\theta = 0 \\
\widetilde{W}_i(\eta,\theta) &= \sum_{m=0}^{M_w}\sum_{n=0}^{N} \widetilde{W}_{i,m,n} T_m^*(\eta)\cos n\theta = 0 \\
\widetilde{U}_{i,\eta}(\eta,\theta) &= \sum_{m=0}^{M_u}\sum_{n=0}^{N} \widetilde{U}_{i,m,n} T_{m,\eta}^*(\eta)\cos n\theta = 0 \\
\widetilde{W}_{i,\eta\eta}(\eta,\theta) &= \sum_{m=0}^{M_w}\sum_{n=0}^{N} \widetilde{W}_{i,m,n} T_{m,\eta\eta}^*(\eta)\cos n\theta = 0
\end{aligned} \qquad \eta = 0,1 \qquad i = 1,2 \qquad (47)$$

where $(\cdot)_{,\eta} = \partial(\cdot)/\partial\eta$ and $(\cdot)_{,\eta\eta} = \partial^2(\cdot)/\partial\eta^2$.

The linear algebraic system given by equations (47) can be solved analytically in terms of coefficients $(\widetilde{U}_{i,1,n}, \widetilde{U}_{i,2,n}, \tilde{V}_{i,0,n}, \tilde{V}_{i,1,n}, \widetilde{W}_{i,0,n}, \widetilde{W}_{i,1,n}, \widetilde{W}_{i,2,n}, \widetilde{W}_{i,3,n})$, for $n \in [0, N]$. Therefore, in the specific case of simply supported DWCNTs, eight different dimensionless coefficients for each SWCNT are derived.

4.3. Rayleigh-Ritz method

In the case of DWCNTs, the maximum number of variables needed to describe a general vibration mode with n circumferential waves is given by $N_p = 2 \times (M_u + M_v + M_w + 3 - p)$, where 2 is the number of concentric SWCNTs, $M_u = M_v = M_w$ is the maximum number of longitudinal half-waves considered and p is the number of equations needed to satisfy the boundary conditions. In the case of simply supported DWCNTs, it is imposed $p = 8$.

Moreover, by means of a specific convergence analysis, it was obtained that $M_u = M_v = M_w = 11$ gives accurate results with relatively reduced computational effort. Therefore, it is found $N_p = 56$.

For a multi-mode vibration analysis including different values of circumferential waves n, the number of degrees of freedom of the system is computed by the relation $N_{\max} = N_p \times (N + 1)$, where N is the maximum number of circumferential waves considered.

Equations (44) are then inserted into the linear expressions of elastic strain energy (27), kinetic energy (32) and van der Waals interaction energy (42) in order to obtain the value of Rayleigh quotient $R(\tilde{\mathbf{q}})$, where $\tilde{\mathbf{q}}$ is a vector containing all the unknown coefficients of expansions (45), which is expressed in

the form [26]:

$$\tilde{\mathbf{q}} = \begin{bmatrix} \vdots \\ \widetilde{U}_{i,m,n} \\ \widetilde{V}_{i,m,n} \\ \widetilde{W}_{i,m,n} \\ \vdots \end{bmatrix} \qquad i = 1,2 \qquad (48)$$

After imposing the stationarity to Rayleigh quotient $R(\tilde{\mathbf{q}})$, the following classic eigenvalue problem in dimensionless form is obtained [26]:

$$\left(-\tilde{\omega}^2\tilde{\mathbf{M}} + \tilde{\mathbf{K}}\right)\tilde{\mathbf{q}} = \mathbf{0} \qquad (49)$$

which provides approximate dimensionless circular frequencies (eigenvalues $\tilde{\omega}_j$) and modal shapes (eigenvectors $\tilde{\mathbf{q}}_j$), with $j = (1,2,\dots,N_{\max})$, where $\tilde{\mathbf{M}}$ and $\tilde{\mathbf{K}}$ are the dimensionless mass and stiffness matrices, respectively.

The approximate modal shape of the j-th mode of the i-th cylindrical shell is provided by expansions (45), where coefficients $(\widetilde{U}_{i,m,n}, \widetilde{V}_{i,m,n}, \widetilde{W}_{i,m,n})$ are replaced with coefficients $(\widetilde{U}^{(j)}_{i,m,n}, \widetilde{V}^{(j)}_{i,m,n}, \widetilde{W}^{(j)}_{i,m,n})$, which are the components of the j-th eigenvector $\tilde{\mathbf{q}}$ of equation (49), and the vector function:

$$\tilde{\mathbf{W}}^{(j)}(\eta,\theta) = \begin{bmatrix} \widetilde{U}_i^{(j)}(\eta,\theta) \\ \widetilde{V}_i^{(j)}(\eta,\theta) \\ \widetilde{W}_i^{(j)}(\eta,\theta) \end{bmatrix} \qquad i = 1,2 \qquad (50)$$

is the approximation of the j-th eigenfunction vector of the original problem.

Eventually, the components of the j-th eigenfunction vector (50) can be normalised by imposing:

$$\max\left[\max\left[\widetilde{U}_i^{(j)}(\eta,\theta), \widetilde{V}_i^{(j)}(\eta,\theta), \widetilde{W}_i^{(j)}(\eta,\theta)\right]\right] = 1 \qquad i = 1,2 \qquad (51)$$

The previous normalization is carried out in order to assign a maximum amplitude equal to the unity to the dominant component of the j-th eigenfunction vector (50), which is the dominant direction of vibration of the j-th modal shape; this normalization improves the computational efficiency.

4.4 Nonlinear vibration analysis

In the nonlinear vibration analysis, the full expressions of elastic strain energy (27) and van der Waals interaction energy (42) are considered (cubic nonlinearity).

The three dimensionless displacements $(\tilde{u}_i, \tilde{v}_i, \tilde{w}_i)$ (44) are re-expanded by adopting the approximate dimensionless modal shapes $(\tilde{U}_i^{(j,n)}, \tilde{V}_i^{(j,n)}, \tilde{W}_i^{(j,n)})$ derived in the previous linear analysis and different dimensionless time laws $(\tilde{f}_{i,u,j,n}, \tilde{f}_{i,v,j,n}, \tilde{f}_{i,w,j,n})$ for each displacement, in the form [51]:

$$\tilde{u}_i(\eta,\theta,\tau) = \sum_{j=1}^{N_u}\sum_{n=1}^{N} \tilde{U}_i^{(j,n)}(\eta,\theta)\tilde{f}_{i,u,j,n}(\tau)$$

$$\tilde{v}_i(\eta,\theta,\tau) = \sum_{j=1}^{N_v}\sum_{n=1}^{N} \tilde{V}_i^{(j,n)}(\eta,\theta)\tilde{f}_{i,v,j,n}(\tau) \qquad i = 1,2 \qquad (52)$$

$$\tilde{w}_i(\eta,\theta,\tau) = \sum_{j=1}^{N_w}\sum_{n=1}^{N} \tilde{W}_i^{(j,n)}(\eta,\theta)\tilde{f}_{i,w,j,n}(\tau)$$

where index j is adopted to order the modes with increasing natural frequency, index n indicates the number of circumferential waves and the dimensionless modal coordinates $(\tilde{f}_{i,u,j,n}, \tilde{f}_{i,v,j,n}, \tilde{f}_{i,w,j,n})$ are unknown time laws to be determined.

Expansions (52) are then inserted into the dimensionless nonlinear expressions of elastic strain energy (27), kinetic energy (32) and van der Waals interaction energy (42).

The dimensionless Lagrange equations of motion, in the case of free vibrations, are written as [52]:

$$\frac{d}{d\tau}\left(\frac{\partial \tilde{T}}{\partial \dot{q}_k}\right) + \frac{\partial(\tilde{U}+\tilde{V})}{\partial q_k} = 0 \qquad k \in [1, N_{\max}] \qquad (53)$$

where $(q_k, \dot{q}_k)$ are the dimensionless Lagrangian coordinates and $N_{\max}$ denotes the maximum number of degrees of freedom of the system, which depends on the number of vibration modes considered in expansions (52).

By substituting the dimensionless vector functions [53]:

$$\mathbf{F}(\mathbf{q}) = \frac{\partial(\tilde{U}+\tilde{V})}{\partial \mathbf{q}} \qquad \mathbf{M}\ddot{\mathbf{q}} = \frac{d}{d\tau}\left(\frac{\partial \tilde{T}}{\partial \dot{\mathbf{q}}}\right) \qquad (54)$$

into the equations (53), where $\mathbf{M}$ is the dimensionless mass matrix and $(\mathbf{q}, \dot{\mathbf{q}}, \ddot{\mathbf{q}})$ are the dimensionless Lagrangian coordinate vectors, we obtain [53]:

$$\mathbf{M}\ddot{\mathbf{q}} + \mathbf{F}(\mathbf{q}) = \mathbf{0} \tag{55}$$

By introducing the vector function $\mathbf{F_x}(\mathbf{q}) = \mathbf{M}^{-1}\mathbf{F}(\mathbf{q})$ into the equation (55), then the dimensionless Lagrange equations of motion for free vibrations are expressed as [53]:

$$\ddot{\mathbf{q}} + \mathbf{F_x}(\mathbf{q}) = \mathbf{0} \tag{56}$$

The dimensionless Lagrange equations of motion (56) denote a set of nonlinear ordinary differential equations; these equations, completed by the modal initial conditions on displacements and velocities, are then solved by considering Runge-Kutta numerical method with suitable accuracy, precision and number of steps.

5. Molecular dynamics simulations of DWCNTs

In the present paper, MD simulations of DWCNTs were performed by using the program developed in the Institute of Mathematical Problems in Biology of the Russian Academy of Sciences (RAS) of Moscow by Professor Nikolai K. Balabaev. In this program, named "PUMA", the AMBER (Assisted Model Building with Energy Refinement) force field is adopted for the modelling of the potential energies, whose constants are measured in Kcal/mol or Kcal/mol·Å^2 in dependence on the kind of interaction, the length is measured in Angstroms (Å), the time in picoseconds (1 ps = 10^{-12} s), the atomic mass in atomic mass units (a.m.u.) and the pressure in GPa. The potential energies used in the MD simulations of DWCNTs are related to the parameters listed below, see Refs. [51-52].

1. Valence bond length L (C-C, sp^2 hybridization), with energy:

$$U_{C-C} = K_1(L - L_0)^2 \tag{57}$$

and constants:

$$K_1 = 480.00 \ \frac{\text{Kcal}}{\text{mol Å}^2}, \qquad L_0 = 1.42 \text{ Å} \tag{58}$$

2. Valence angle θ (C-C-C, sp^2 hybridization), with energy:

$$U_{C-C-C} = K_2(\theta - \theta_0)^2 \tag{59}$$

and constants:

$$K_2 = 90.00 \ \frac{\text{Kcal}}{\text{mol}}, \qquad \theta_0 = 120^{\circ} \tag{60}$$

3. Torsion angle φ (C-C-C-C, sp^2 hybridization), which represents the "dihedral" interaction. There are two different types of this interaction.
    a. The first is associated with the so-called "proper" dihedral angle, with energy:

$$U_{pr} = K_3(1 - \cos 2\varphi) \tag{61}$$

and constant:

$$K_3 = 3.0\ \frac{\text{Kcal}}{\text{mol}} \tag{62}$$

b. The second is associated with the so-called "improper" dihedral angle, with energy:

$$U_{impr} = K_4(1 - \cos 2\varphi) \tag{63}$$

and constant:

$$K_4 = 0.37\ \frac{\text{Kcal}}{\text{mol}} \tag{64}$$

4. Van der Waals interactions, which are calculated for the carbon atoms that are not coupled by valence bonds. Van der Waals interactions are described by Lennard-Jones pair potential:

$$U_{vdW} = 4\varepsilon\left(\left(\frac{\sigma}{r}\right)^{12} - \left(\frac{\sigma}{r}\right)^{6}\right) \tag{65}$$

with constants:

$$\varepsilon = 0.086\ \frac{\text{Kcal}}{\text{mol}}, \qquad \sigma = 3.816\ \text{Å} \tag{66}$$

Since van der Waals interactions are long-range enough, then the cutting radius $R = 10.5$ Å is adopted to restrict their domain.

The typical procedure of MD simulations consists of three consecutive stages.

I. The first stage is the *initialization*. The initially built object is simulated during approximately 20 ps at the thermostat temperature $T = 100$ K. The thermostat is of collision-type. The bath of the virtual particles with fixed mass and kinetic energy collides with the atoms of the CNTs. The frequency of collisions and the mass of thermostat particles can be varied: in this work, a frequency ~ 10 collisions per ps and a mass of thermostat particles ~ 0.5 a.m.u. are adopted.

II. The second stage is the *relaxation*. Usually, the thermostat temperature is increased up to $300\ K$ and then it is waited for approximately 100 ps, until the stabilization of the main parameters of the DWCNT, i.e., temperature T, density ρ, unit cell dimensions (A_x, A_y, A_z) and pressure components (P_x, P_y, P_z), is obtained.

III. The third stage consists in the *deformation* of the CNTs. A priori, the required circumferential and longitudinal wave numbers and the amplitude of the deformation are set. During this stage the external field is applied to the CNTs and it is waited for until the relaxation to the deformed shape is finished. During this stage the temperature is preserved at $T = 300\ K$. As usual, this stage is finished after ~ 100 ps. An additional procedure may be applied for the cooling of the deformed CNT. Usually, the cooling rate is ~ 2 K per ps. However, it is not mandatory.

The measurement of the oscillation frequencies assumes the conservation of the energy. Therefore, the thermostat is turned off at the start of this stage. As a rule, zero masses of the thermostat particles are assumed. Simultaneously, the external field is turned off. Naturally, since the deformation shape of the CNT is not absolutely accurate for the discrete system, some redundant displacements of the atoms can be observed. Therefore, the measurement is started 3-5 ps later. Then, the velocities of the atoms during approximately 150-200 ps are recorded in the trajectory file.
Two approaches may be used to obtain the frequency spectrum.

A. The first approach consists in the analysis of the correlation function velocity-velocity along the trajectory. The Fourier spectrum of the function displays only the main frequency of the system (partial spectrum). This results in a long and very expensive procedure.
B. The second approach assumes that the frequency spectrum of the system contains all the most relevant motions of the object under consideration. If the system has been initially deformed in approximately correct state, then the most important oscillations will be well distinguished within the spectrum (total spectrum).

Actually, the MD simulation results reported in the present work have been obtained by considering in some cases the first and in other cases the second approach, based on the computational effort.

6. Numerical results

In the present paper, the vibrations of a simply supported armchair DWCNT with chirality indices $(r_1, s_1) = (20,20)$ for the inner SWCNT and $(r_2, s_2) = (25,25)$ for the outer SWCNT are analysed. By adopting relation (19), these chirality indices provide radius $R_1 = 1.356$ nm for the inner SWCNT and radius $R_2 = 1.695$ nm for the outer SWCNT, respectively. Geometric parameters of the DWCNT are completed by equivalent thickness $h = 0.066$ nm [26] and length $L = 12.17$ nm of the SWCNTs, see Table 1.

The previous configuration for the DWCNT was selected on the basis of three considerations.

1) The difference between the radii of the two concentric SWCNTs composing this DWCNT is equal to 0.34 nm, and "a MWCNT consists of two or more concentric cylindrical shells of graphene sheets arranged coaxially around a central hollow with interlayer separation as in graphite (0.34 nm)" [40]. Therefore, the DWCNT of Table 1 is realistic.

2) In the elastic shell model, assuming the equivalent thickness $h = 0.066$ nm [26], it is found that the thickness ratios of the inner SWCNT ($R_1/h = 20.54$) and of the outer SWCNT ($R_2/h = 25.68$) are both comprised within the range of validity of the thin shell theories ($20 \leq R/h \leq 500$), see Ref. [21], where the first Kirchhoff-Love's assumption is verified (i.e., the thickness is small if compared with the radius of curvature of the middle surface of the shell). Therefore, the DWCNT of Table 1 can be studied by adopting Sanders-Koiter thin shell theory.

3) By considering the discrete nature of CNTs, and assuming the geometric parameters of Table 1, it is found for the DWCNT a total number of carbon atoms (9986) very close but however lower than the maximum number (10000) tractable by the MD simulation program packet PUMA adopted in this work.

In particular, the DWCNT length $L = 12.17$ nm corresponds to 50 C-C bond rings, where the axial distance between two rings of C-C atoms in the case of armchair SWCNTs is $d = 0.246$ nm.

Inner radius R_1 [nm]	1.356
Outer radius R_2 [nm]	1.695
Equivalent thickness h [nm]	0.066
Length L [nm]	12.17

Table 1. Geometric parameters of the considered simply supported armchair DWCNT

6.1. Local anisotropic elastic shell model

In Table 2, the values of carbon-carbon (C-C) bond parameters (a, K_ρ, K_θ), C-C distance parameters (ε, σ) and material parameters (Y, ρ) of CNTs retrieved from the literature are listed.

In particular parameters K_ρ and K_θ, which denote force constants related to the variance of C-C bond length and angle, respectively, were derived from experimental data of graphite and are used in the anisotropic "stick-spiral model" that is based on the molecular mechanics approach, see Refs. [28-29] for the details.

Moreover, in the present paper, van der Waals interaction forces between the layers of the DWCNT are modelled by adopting Taylor expansion of Lennard-Jones pair potential (34), considering C-C bond length a, C-C potential depth ε and C-C equilibrium separation distance σ [40].

Finally, in order to study the actual discrete DWCNT as a couple of concentric equivalent continuous thin cylindrical shells, a reference dimensional surface elastic constant Y (30) and an equivalent mass density ρ, resulting from surface density of graphite $\sigma = \rho h = 7.718 \times 10^{-7}$ kg/m^2, are used [26].

C-C bond parameters [28-29]	
C-C bond length a [nm]	0.142
C-C bond elongation K_ρ [nN/nm]	742
C-C bond angle variance K_θ [nN · nm]	1.42
C-C distance parameters [40]	
C-C potential depth ε [10^{-22} J]	4.755
C-C equilibrium separation distance σ [nm]	0.3407
CNT material parameters [26]	
Surface elastic constant Y [N/m]	285.6
Mass density ρ [kg/m^3]	11700

Table 2. Mechanical parameters of the considered simply supported armchair DWCNT

In Table 3, the lowest natural frequencies of a simply supported armchair DWCNT with the geometric parameters of Table 1 and the mechanical parameters of Table 2 are listed. These natural frequencies are obtained by using Sanders-Koiter shell theory and local ($e_0 = 0$) anisotropic elastic shell model (the proper value of nonlocal parameter e_0 will be calibrated by means of comparisons with data from molecular dynamics simulations). The radial displacement w is considered (i.e. natural frequencies related to modal shapes with prevalent radial component W). Bending ($n = 1$) and circumferential flexure ($n = 2$) modes are investigated (they are the modes with the lowest natural frequencies). From Table 3 it can be seen that, both for bending and for circumferential flexure modes, the prevalent radius (i.e. the radius providing the highest radial displacement w) always corresponds to R_1 (inner SWCNT). Moreover, the fundamental mode (i.e. the mode with the lowest natural frequency) is $(1,2)$.

Mode (m,n)	Displacement (u,v,w)	Radius (R_1,R_2)	Natural frequency f [THz]
(1,2)	w	R_1	0.26122
(2,2)	w	R_1	0.62898
(1,1)	w	R_1	0.73878
(3,2)	w	R_1	0.84648
(2,1)	w	R_1	1.29156
(4,2)	w	R_1	1.35412
(5,2)	w	R_1	1.51207
(3,1)	w	R_1	1.53321
(6,2)	w	R_1	1.65061
(4,1)	w	R_1	1.78831
(7,2)	w	R_1	1.83847
(5,1)	w	R_1	1.94160
(6,1)	w	R_1	2.06526

Table 3. Natural frequencies of the simply supported armchair DWCNT of Table 1. Local anisotropic elastic shell model with mechanical parameters of Table 2. Bending modes ($n = 1$). Circumferential flexure modes ($n = 2$)

6.2. Molecular dynamics simulations

In the present Section, the results from MD simulations carried out on a simply supported armchair DWCNT with the geometric parameters of Table 1, by taking into account the force field parameters and applying the procedure stages described in Section 5, are reported.

In particular, the DWCNT is simulated by means of two concentric isolated SWCNTs with van der Waals interaction forces between the layers and periodic (i.e. simply supported) boundary conditions along the SWCNT axis.

In Figure 3 the initialization of the DWCNT, which is the first stage of MD simulations, is illustrated. During this initial stage, the DWCNT remains undeformed (no longitudinal or circumferential wave) and is subjected to the constant thermostat temperature $T = 100$ K.

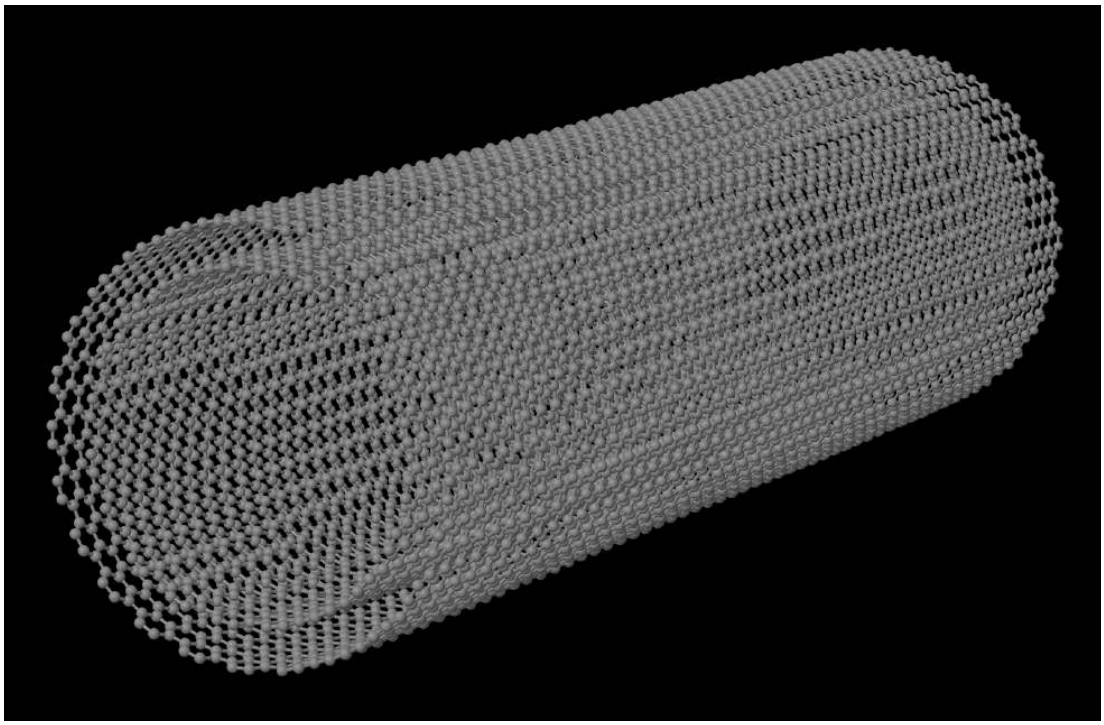

Figure 3. Initialization of the DWCNT at thermalized state ($T = 100$ K)

By considering the results from the local anisotropic elastic shell model reported in Section 6.1, the first MD simulations are performed for the circumferential flexure mode $(1,2)$, which has $m = 1$ longitudinal half-wave and $n = 2$ circumferential waves (it is the fundamental mode in the continuum modelling, i.e., the vibration mode with the lowest natural frequency).

In Figure 4, the circumferential flexure deformation of the DWCNT with $(m, n) = (1,2)$, under radial deformation amplitude $\delta w = 0.1$ nm and constant temperature $T = 300$ K, is shown.

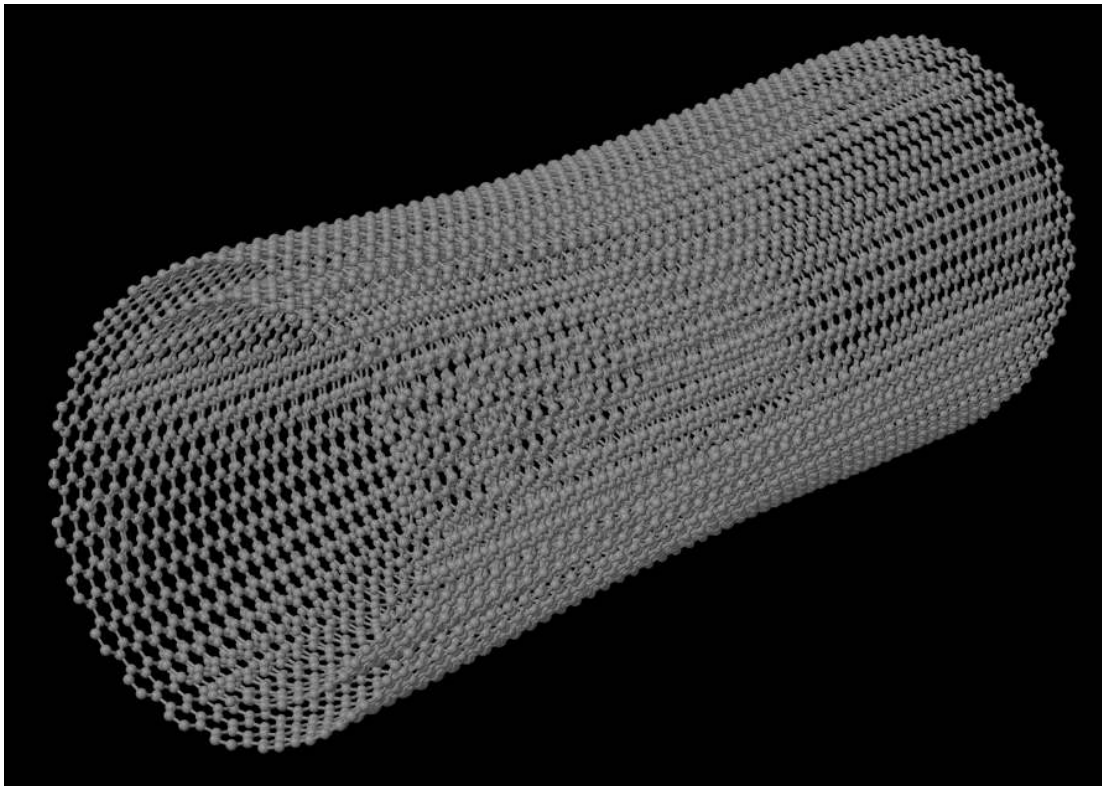

Figure 4. Circumferential flexure deformation of the DWCNT with $(m, n) = (1,2)$

In this case, in order to obtain the frequency spectrum, velocity-velocity correlation function along the trajectory was studied (see the first approach described in Section 5). In Figure 5, Fourier spectrum of the autocorrelation function $< v_j(0)\ v_j(t) >$, which displays the frequency corresponding to the circumferential flexure deformation $(m, n) = (1,2)$, is shown, where the CFM oscillation frequency is $f_{1,2} \approx 2.5 \times 10^{11}$ Hz.

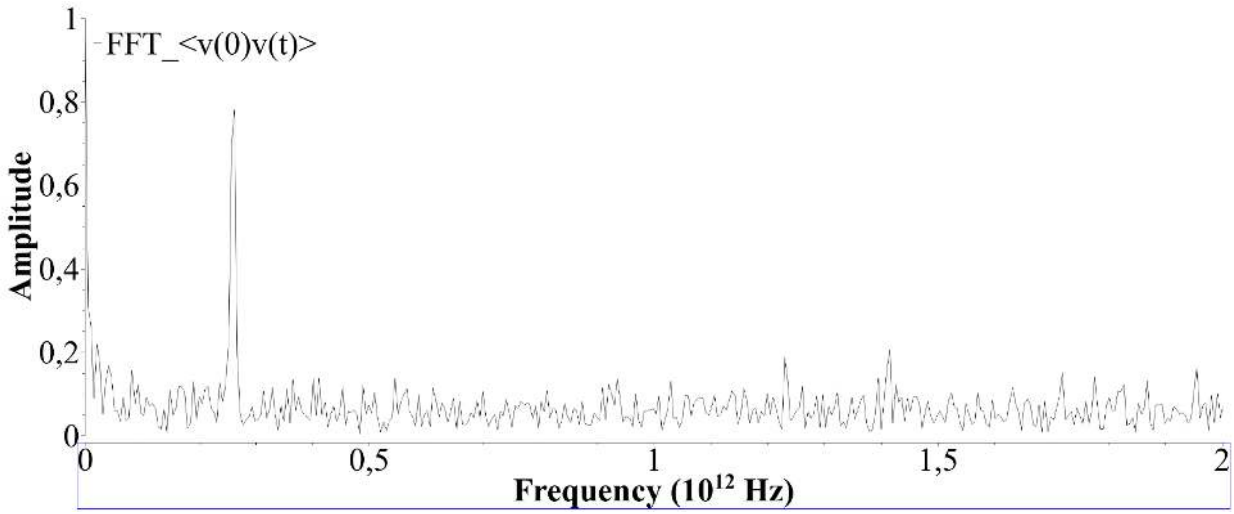

Figure 5. Frequency spectrum of the circumferential flexure deformed DWCNT with $(m, n) = (1,2)$

In this specific case, an additional procedure was applied for the cooling of the circumferential flexure deformed DWCNT from $T = 300$ K to $T = 100$ K in the time interval from $t = 20$ ps to $t = 100$ ps with cooling rate $dT/dt = 2.5$ K/ps, see Figure 6, where the measurement of the oscillation natural frequencies is actually performed at 160 K.

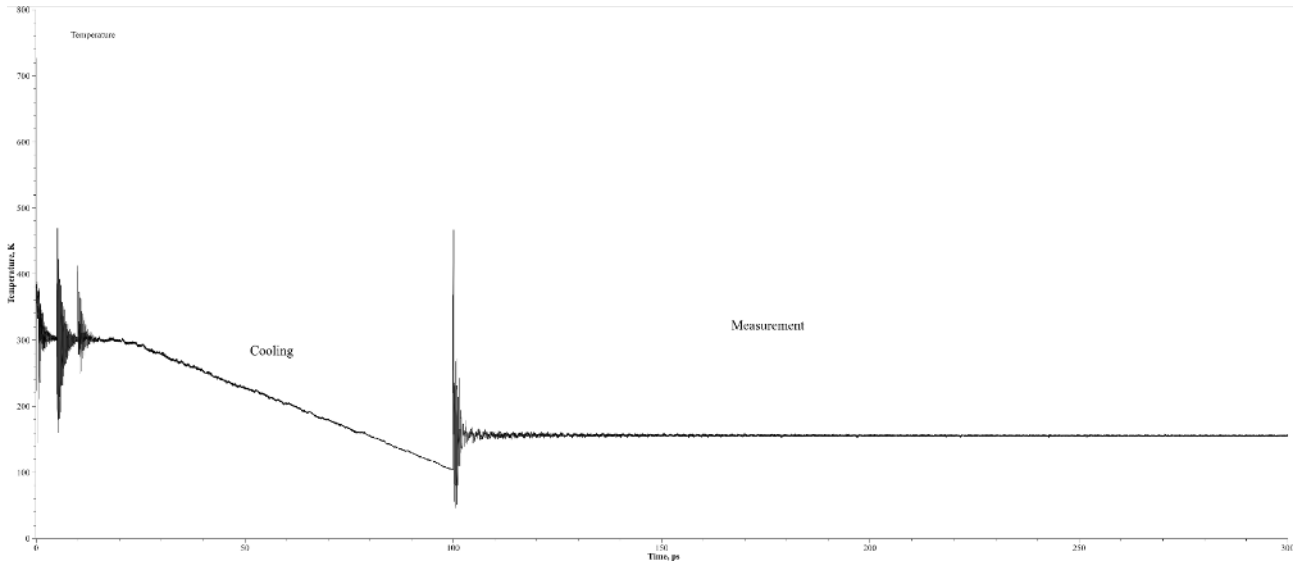

Figure 6. Cooling procedure of the circumferential flexure deformed DWCNT with $(m, n) = (1,2)$

The same procedure is performed for the MD simulations of the DWCNT in case of circumferential flexure mode $(2,2)$, with $m = 2$ longitudinal half-waves and $n = 2$ circumferential waves (it is the mode with the second lowest natural frequency in the continuum modelling of Section 6.1). In Figure 7, Fourier spectrum of the autocorrelation function $< v_j(0)\ v_j(t) >$ for the circumferential flexure deformation $(m, n) = (2,2)$ is shown, where the CFM oscillation frequency is $f_{2,2} \approx 6.0 \times 10^{11}$ Hz.

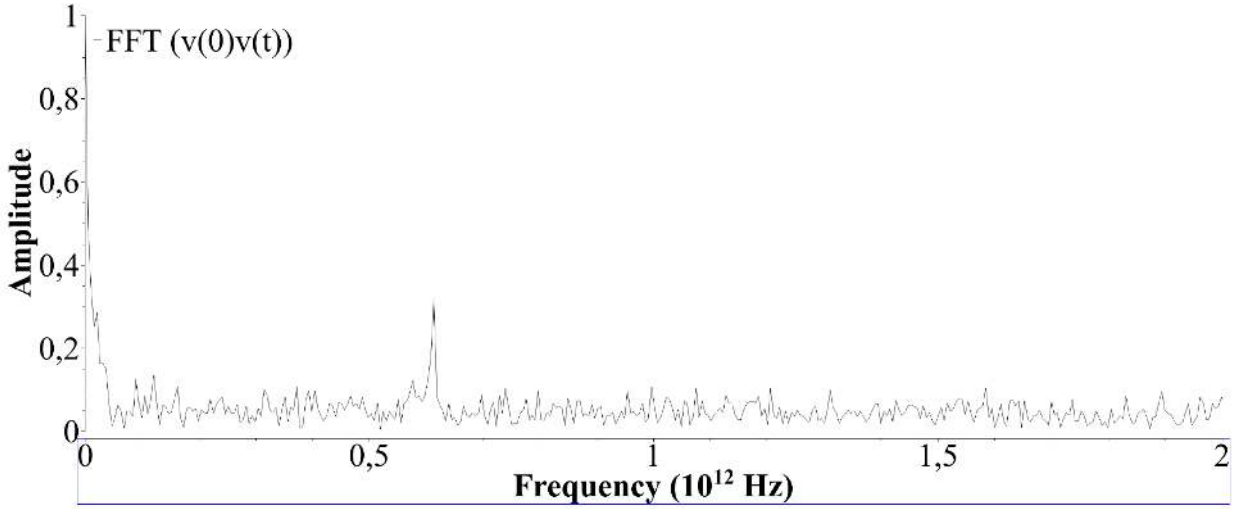

Figure 7. Frequency spectrum of the circumferential flexure deformed DWCNT with $(m, n) = (2,2)$

Let us consider the MD simulations of the DWCNT in the case of circumferential flexure mode (3,2), which presents $m = 3$ longitudinal half-waves and $n = 2$ circumferential waves.
In Figure 8, the circumferential flexure deformation of the DWCNT with $(m, n) = (3,2)$, under radial deformation amplitude $\delta w = 0.1$ nm and constant temperature $T = 100$ K, is shown.

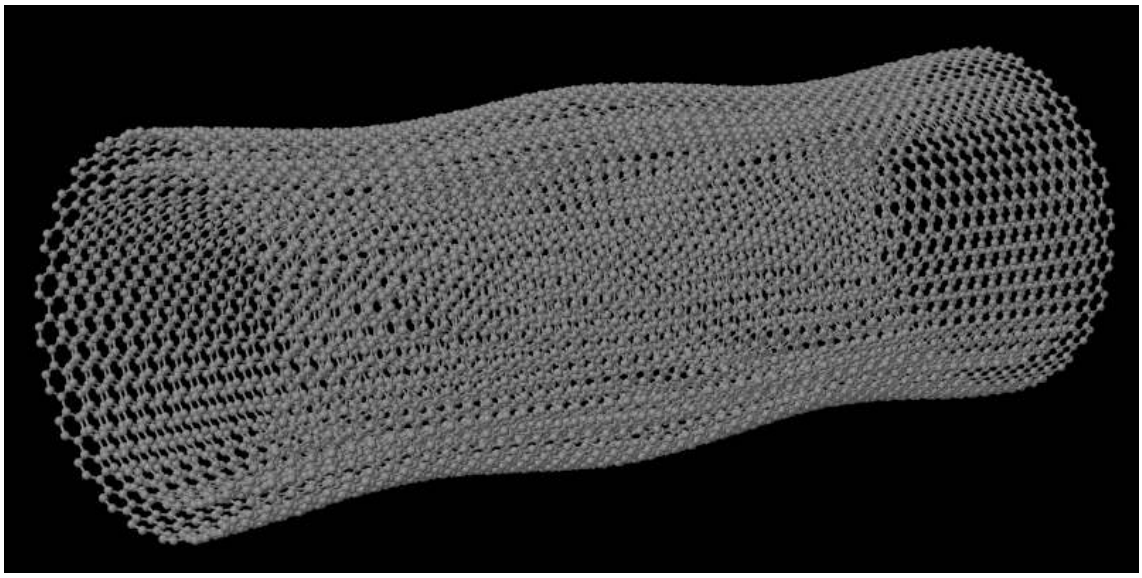

Figure 8. Circumferential flexure deformation of the DWCNT with $(m, n) = (3,2)$

In this case, in order to obtain a frequency spectrum containing all the CFM natural frequencies, it is adopted the second approach reported in Section 5, i.e., the Fourier transform of the average square of the atom velocities is performed to obtain the FFT spectrum of the kinetic energy, see Figure 9.

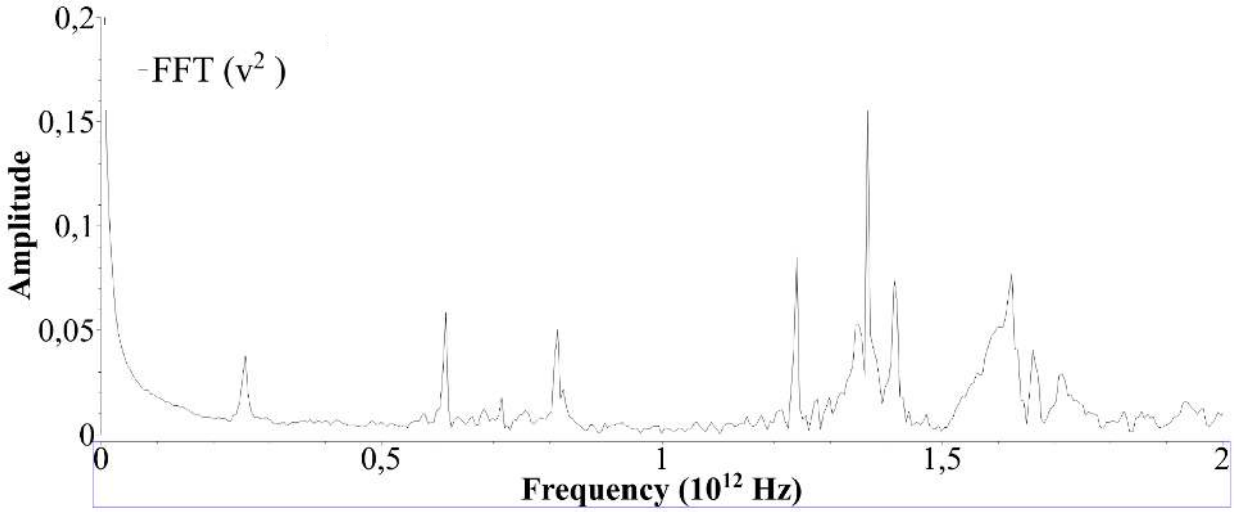

Figure 9. Frequency spectrum with all the CFM natural frequencies (deformation mode (3,2))

From Figure 9, the following CFM natural frequencies $f_{1,2} \approx 2.5 \times 10^{11}$ Hz, $f_{2,2} \approx 6.0 \times 10^{11}$ Hz, $f_{3,2} \approx 8.0 \times 10^{11}$ Hz, $f_{4,2} \approx 1.25 \times 10^{12}$ Hz, $f_{5,2} \approx 1.35 \times 10^{12}$ Hz and $f_{6,2} \approx 1.40 \times 10^{12}$ Hz can be clearly distinguished within the spectrum.

A similar "total spectrum" can be obtained by computing Fourier transform of the average square of the atom velocities of the DWCNT in the case of circumferential flexure deformation with $(m, n) = (1,2)$ (see Figure 4), whose "partial spectrum" was reported in Figure 5.

In Figure 10 the FFT spectrum of the kinetic energy of the DWCNT for the CFM $(1,2)$ is shown; the same CFM natural frequencies of Figure 9, i.e., $f_{1,2} \approx 2.5 \times 10^{11}$ Hz, $f_{2,2} \approx 6.0 \times 10^{11}$ Hz, $f_{3,2} \approx 8.0 \times 10^{11}$ Hz, $f_{4,2} \approx 1.25 \times 10^{12}$ Hz, $f_{5,2} \approx 1.35 \times 10^{12}$ Hz and $f_{6,2} \approx 1.40 \times 10^{12}$ Hz are clearly distinguished also within this spectrum.

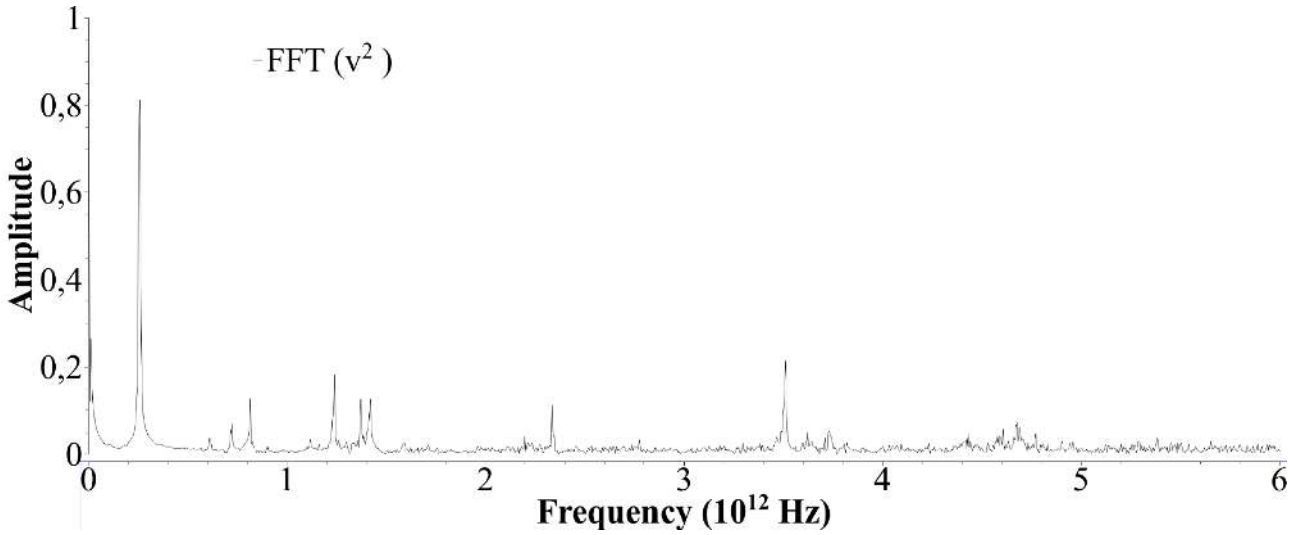

Figure 10. Frequency spectrum with all the CFM natural frequencies (deformation mode (1,2))

However, in the frequency spectrum shown in Figure 10 there is a peak at the natural frequency $f \approx 7.0 \times 10^{11}$ Hz with relatively high amplitude that is not present in the frequency spectrum of Figure 9 and therefore should be investigated.

Since, from Table 3, it is derived that the vibration mode with natural frequency $f \approx 7.0 \times 10^{11}$ Hz is the bending mode $(m, n) = (1,1)$, with $m = 1$ longitudinal half-wave and $n = 1$ circumferential wave, then MD simulations were performed also on this mode.

In Figure 11, the bending deformation of the DWCNT with $(m, n) = (1,1)$, under radial deformation amplitude $\delta w = 0.1$ nm and constant temperature $T = 100$ K, is shown. In Figure 12, the frequency spectrum of the DWCNT for the bending mode $(1,1)$, obtained by computing the Fourier transform of the average square of the atom velocities (i.e. "total spectrum" of the kinetic energy), is reported.

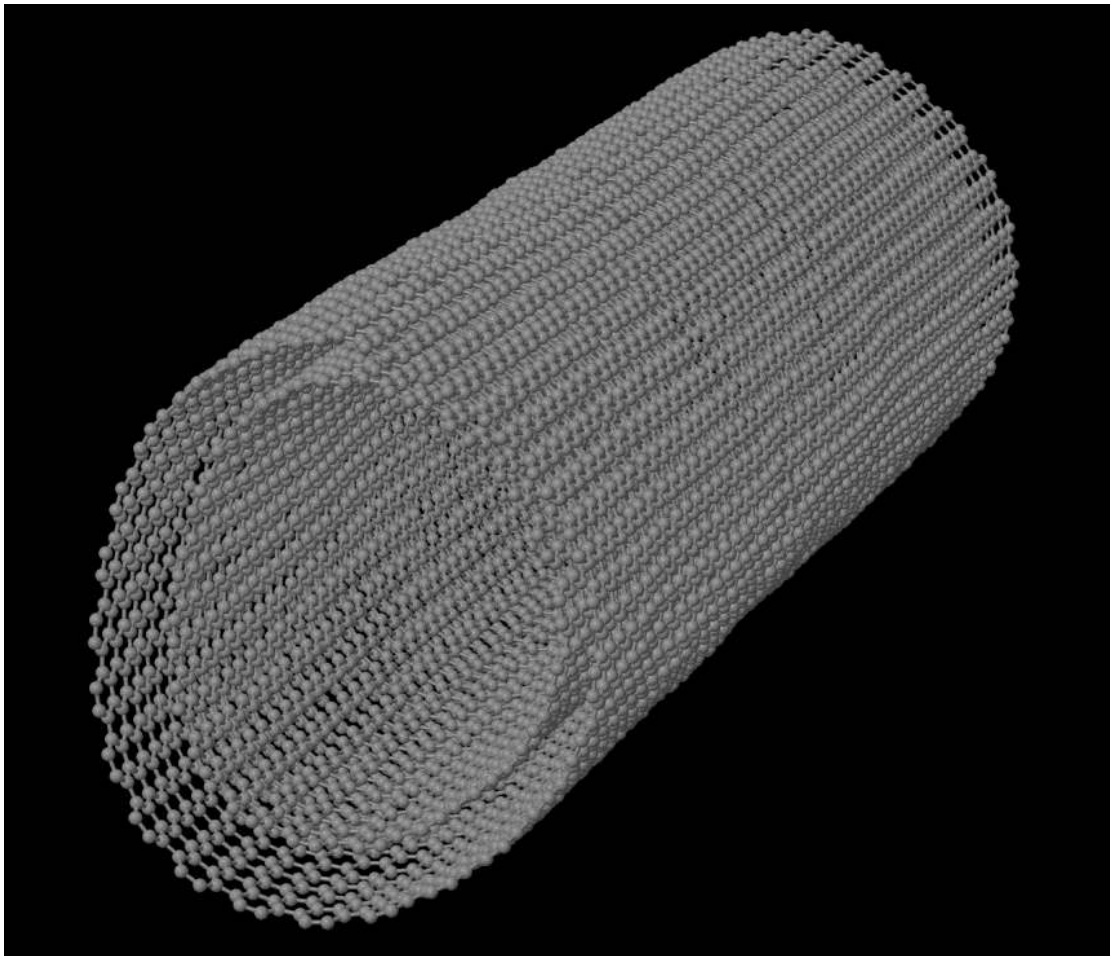

Figure 11. Bending deformation of the DWCNT with $(m, n) = (1,1)$

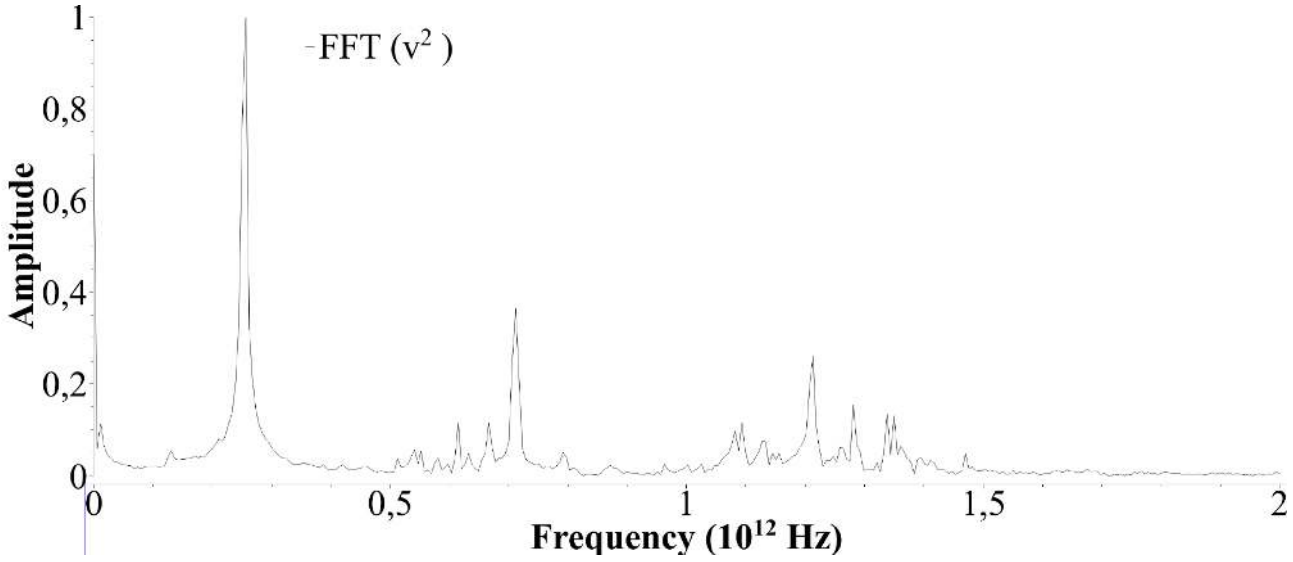

Figure 12. Frequency spectrum with all the BM natural frequencies (deformation mode (1,1))

From Figure 12, it can be clearly distinguished the natural frequency $f \approx 2.5 \times 10^{11}$ Hz, which is related to the CFM $(1,2)$, and the natural frequencies $f \approx 7.0 \times 10^{11}$ Hz and $f \approx 1.2 \times 10^{12}$ Hz, which are related to the bending modes $(1,1)$ and $(2,1)$.

Since within the frequency spectrum with all the BM natural frequencies of Figure 12 it appears also the natural frequency of the CFM $(1,2)$ with the highest amplitude peak, then it can be concluded that there is a strong resonance interaction between circumferential flexure $(1,2)$ and bending $(1,1)$ modes.

The results of the MD simulations for the natural frequencies of bending $(n = 1)$ and circumferential flexure $(n = 2)$ modes are reported in Table 4, where the fundamental mode (i.e. the vibration mode with the lowest natural frequency) is again the CFM $(1,2)$.

Mode (m, n)	Natural frequency f [THz]
(1,2)	0.25
(2,2)	0.60
(1,1)	0.70
(3,2)	0.80
(2,1)	1.20
(4,2)	1.25
(5,2)	1.35
(6,2)	1.40

Table 4. Natural frequencies of the simply supported armchair DWCNT of Table 1. Molecular dynamics simulations with potential energy parameters of Section 5. Bending modes $(n = 1)$. Circumferential flexure modes $(n = 2)$

6.3. Calibration of the nonlocal parameter

In the present Section, the natural frequencies, obtained from the local anisotropic elastic shell model of Section 6.1, are compared with the ones from the MD simulations of Section 6.2. The goal is to get the proper value of the nonlocal parameter e_0 to be inserted into the constitutive equations (5) of the nonlocal anisotropic elastic shell model.

In Table 5, the natural frequencies of the simply supported armchair DWCNT of Table 1, obtained by means of the local ($e_0 = 0$) anisotropic elastic shell model (see Table 3), are compared with the ones obtained via MD simulations (see Table 4). Bending modes (BMs) and circumferential flexural modes (CFMs) are considered.

Mode (m, n)	Natural frequency f [THz]		Difference %
	Local anisotropic elastic shell model	Molecular dynamics simulations	
(1,2)	0.26122	0.25	4.49
(2,2)	0.62898	0.60	4.83
(1,1)	0.73878	0.70	5.54
(3,2)	0.84648	0.80	5.81
(2,1)	1.29156	1.20	7.63
(4,2)	1.35412	1.25	8.33
(5,2)	1.51207	1.35	12.0
(6,2)	1.65061	1.40	17.9

Table 5. Natural frequencies of the simply supported armchair DWCNT of Table 1. Comparisons between local ($e_0 = 0$) anisotropic elastic shell model (see Table 3) and molecular dynamics simulations (see Table 4)

From Table 5, the following observations can be made:

- the local anisotropic elastic shell model overestimates the natural frequencies compared to the MD simulations both for BMs and for CFMs;
- considering the same number of circumferential waves n, the overestimation increases as the number of longitudinal half-waves m increases;

- considering the same number of longitudinal half-waves m, the overestimation decreases as the number of circumferential waves n increases (the overestimation is higher for BMs than for CFMs).

The calibration of the nonlocal parameter e_0 is performed by inserting different values of e_0 into the constitutive equations (5) of the nonlocal anisotropic elastic shell model until the natural frequency of the fundamental (i.e. the lowest frequency) mode (1,2) becomes equal to the one of the same mode obtained via MD simulations: from this iterative calibration procedure we obtained the nonlocal parameter $e_0 = 2$, which gives $f_{1,2} = 0.25028$ THz ≈ 0.25 THz (the fundamental natural frequency of the nonlocal model coincides with the one from MD simulations).
Once we calibrated the nonlocal parameter and inserted its value into the constitutive equations (5), the natural frequencies of the nonlocal anisotropic elastic shell model are obtained, and they are reported in Table 6 together with the natural frequencies derived from MD simulations.

Mode (m,n)	Natural frequency f [THz]		Difference %
	Nonlocal anisotropic elastic shell model	Molecular dynamics simulations	
(1,2)	0.25028	0.25	0.11
(2,2)	0.60378	0.60	0.63
(1,1)	0.70567	0.70	0.81
(3,2)	0.81192	0.80	1.49
(2,1)	1.22796	1.20	2.33
(4,2)	1.29050	1.25	3.24
(5,2)	1.40495	1.35	4.07
(6,2)	1.48316	1.40	5.94

Table 6. Natural frequencies of the simply supported armchair DWCNT of Table 1. Comparisons between nonlocal ($e_0 = 2$) anisotropic elastic shell model and molecular dynamics simulations

From Tables 5-6, the following comments can be made:

- the natural frequencies reduce from the local to the nonlocal anisotropic elastic shell model both for BMs and for CFMs;
- in the nonlocal anisotropic elastic shell model, the natural frequencies reduce as the value of the nonlocal parameter e_0 increases both for BMs and for CFMs;
- considering the same number of circumferential waves n, the reduction increases as the number of longitudinal half-waves m increases;
- considering the same number of longitudinal half-waves m, the reduction decreases as the number of circumferential waves n increases (the reduction is higher for BMs than for CFMs).

By comparing Tables 5-6, we note that the nonlocal anisotropic elastic shell model predicts the natural frequencies that are lower than the local model, moreover, the natural frequencies decrease with the increasing of the nonlocal parameter. This behaviour is due to the fact that the nonlocal elasticity theory [33] introduces a flexible model, in which a SWCNT is viewed as a system of carbon atoms connected by elastic springs, while the local elasticity theory [21] considers infinitely rigid springs between the carbon atoms: as a physical consequence, the nonlocal model has frequency reduction.

6.4. Nonlinear vibrations of DWCNTs

In the present Section, nonlinear vibrations of a simply supported armchair DWCNT with geometric parameters of Table 1 and mechanical parameters of Table 2 are investigated by adopting the nonlocal anisotropic elastic shell model with the nonlocal parameter $e_0 = 2$.

Nonlinear modal expansions in the terms of approximate linear modal shapes and different nonlinear time laws (i.e. modal coordinates) for each displacement of the two SWCNTs are adopted.

It was demonstrated that the nonlinear modal expansions including the directly excited (i.e. subjected to relatively high modal initial conditions) mode, one asymmetric and one axisymmetric mode (8dof model), are able to predict with sufficient accuracy the nonlinear behaviour of SWCNTs, see Refs. [51-52] for more details.

Therefore, in the present work, it is assumed that the following nonlinear modal expansions for the two SWCNTs, which include the vibration modes (1,2), (2,2) and (1,0) (16 dof model), are able to properly predict the nonlinear behaviour of the considered DWCNT:

$$\tilde{u}_i(\eta,\theta,\tau) = \tilde{U}_i^{(1,2)}(\eta,\theta)\tilde{f}_{i,u,1,2}(\tau) + \tilde{U}_i^{(2,2)}(\eta,\theta)\tilde{f}_{i,u,2,2}(\tau) + \tilde{U}_i^{(1,0)}(\eta,\theta)\tilde{f}_{i,u,1,0}(\tau)$$

$$\tilde{v}_i(\eta,\theta,\tau) = \tilde{V}_i^{(1,2)}(\eta,\theta)\tilde{f}_{i,v,1,2}(\tau) + \tilde{V}_i^{(2,2)}(\eta,\theta)\tilde{f}_{i,v,2,2}(\tau) \qquad i = 1,2 \qquad (67)$$

$$\widetilde{w}_i(\eta,\theta,\tau) = \widetilde{W}_i^{(1,2)}(\eta,\theta)\tilde{f}_{i,w,1,2}(\tau) + \widetilde{W}_i^{(2,2)}(\eta,\theta)\tilde{f}_{i,w,2,2}(\tau) + \widetilde{W}_i^{(1,0)}(\eta,\theta)\tilde{f}_{i,w,1,0}(\tau)$$

In the present nonlinear analysis, no modal initial conditions are imposed on the velocities; on the other hand, increasing modal initial conditions on the displacements of the mode (1,2), which is the directly excited mode, and constant modal initial conditions on the displacements of the asymmetric (2,2) and axisymmetric (1,0) modes, are applied, see Table 7.

Case	$\tilde{f}_{i,u,1,2}(0) = \tilde{f}_{i,v,1,2}(0) = \tilde{f}_{i,w,1,2}(0)$	$\tilde{f}_{i,u,2,2}(0) = \tilde{f}_{i,u,1,0}(0) = \tilde{f}_{i,v,2,2}(0) = \tilde{f}_{i,w,2,2}(0) = \tilde{f}_{i,w,1,0}(0)$
A	1.0×10^{-2}	1.0×10^{-4}
B	1.0×10^{-1}	1.0×10^{-4}
C	2.0×10^{-1}	1.0×10^{-4}
D	3.0×10^{-1}	1.0×10^{-4}
E	4.0×10^{-1}	1.0×10^{-4}
F	5.0×10^{-1}	1.0×10^{-4}

Table 7. Dimensionless modal initial conditions imposed on the displacements in the nonlinear modal expansions (67)

6.4.1. Linear van der Waals interaction forces

In this part, the full expression of the elastic strain energy (27) (i.e. linear and nonlinear terms) and the linear expression of van der Waals interaction energy (42) (i.e. only linear terms) are considered, where the dimensionless pressure $\tilde{p}_i$ (38) is expressed in linear form as:

$$\tilde{p}_i(\eta,\theta) = \tilde{c}_{ij}\left(\delta_i\widetilde{w}_i - \delta_j\widetilde{w}_j\right) \qquad i,j = 1,2 \qquad i \neq j \qquad (68)$$

In Figure 13, the time histories of the dimensionless radial modal coordinate $\tilde{f}_{1,w,1,2}(\tau)$ of the inner SWCNT related with the directly excited mode (1,2) under the increasing dimensionless modal initial conditions $\tilde{f}_{1,w,1,2}(0)$ of Table 7 are shown. From this Figure it is noted that, by increasing the value of the dimensionless modal initial conditions, the behaviour of the dimensionless modal coordinate changes from linear (cases A,B,C) to nonlinear (cases D,E,F), where the periodicity is absent, and the maximum amplitude of the response increases.

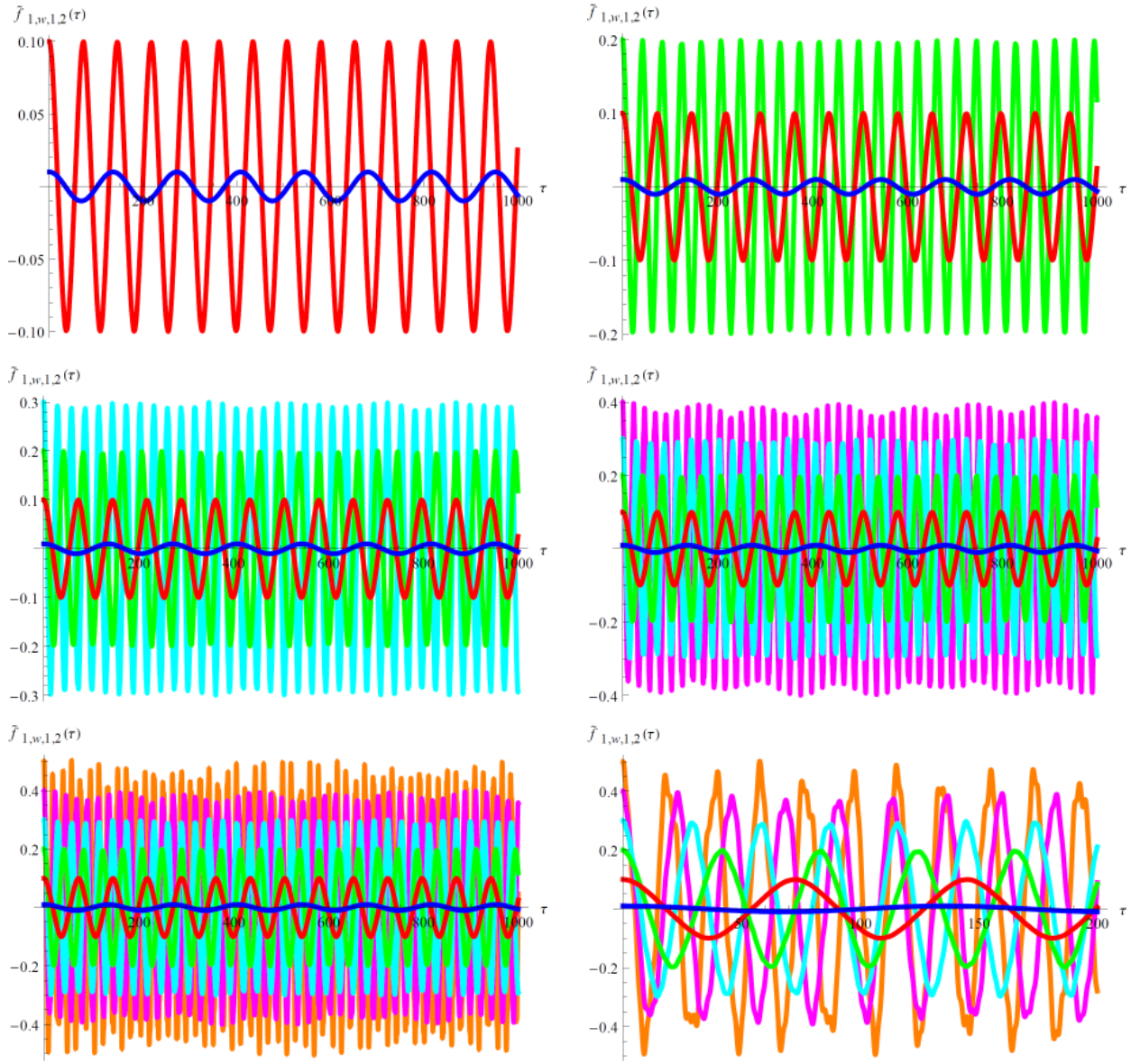

Figure 13. Time histories of the dimensionless modal coordinate $\tilde{f}_{1,w,1,2}(\tau)$ under increasing modal initial conditions of Table 7. —: Case A. —: Case B. —: Case C. —: Case D. —: Case E. —: Case F.

Starting from the time histories reported in Figure 13, by sampling them at regular time steps, we can first obtain the fast Fourier transform (FFT) of the sampled data with an appropriate choice of Fourier parameters, as an integral in the time, and then, once defined a set of frequency values able to provide abscissae for the spectral values, we can plot the corresponding frequency spectra.

By considering the spectra derived for the different increasing values of modal initial conditions, and computing frequency and amplitude of the main peak, we can build the corresponding dimensionless amplitude-frequency response, in the form of a backbone curve, see Figure 14.

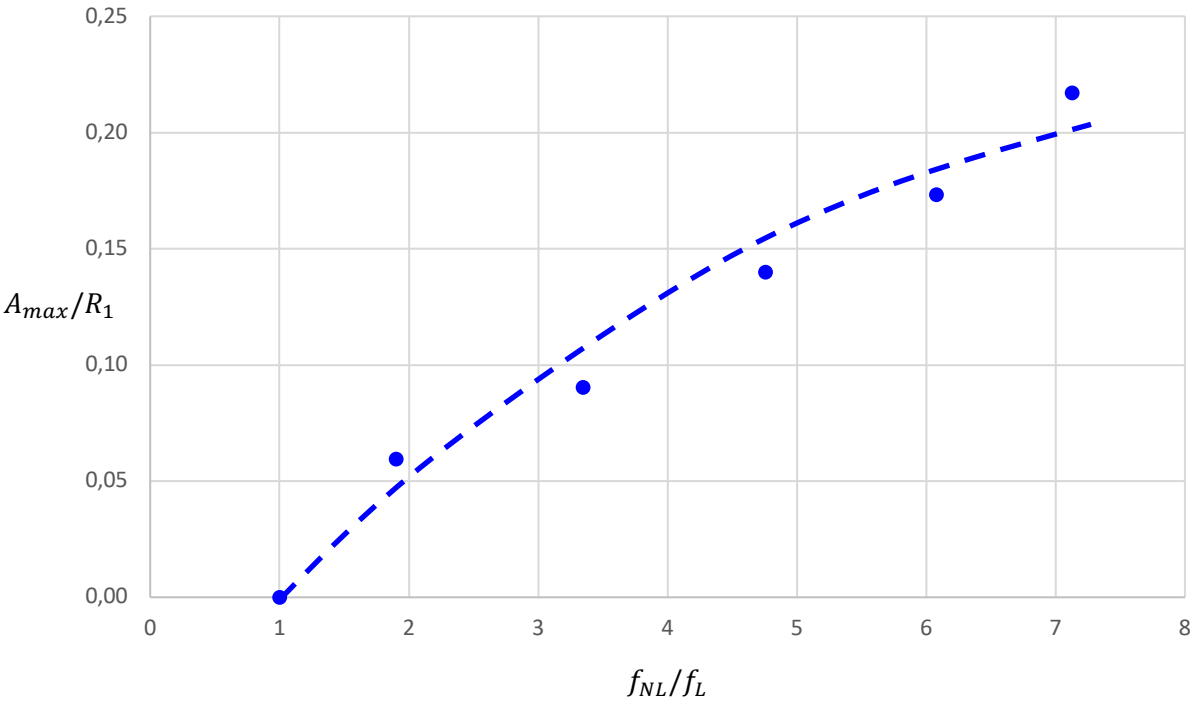

Figure 14. Nonlinear amplitude-frequency curve of the simply supported armchair DWCNT of Table 1. Initially excited mode (1,2) with increasing modal initial conditions of Table 7. Linear van der Waals interaction energy

In the dimensionless amplitude-frequency curve represented in Figure 14, f_{NL}/f_L is the ratio between the nonlinear and linear natural frequency of the initially excited mode (1,2), where the linear natural frequency is constant ($f_L = 0.25028$ THz) and the nonlinear natural frequency f_{NL} is a function of the increasing modal initial conditions imposed, while A_{max}/R_1 is the ratio between the maximum amplitude A_{max} of the corresponding response and the radius R_1 of the inner SWCNT.

From Figure 14 it can be noted that the nonlinear response of the considered DWCNT is hardening: this confirms the results obtained for cylindrical shells in Refs. [49-50], that is, in case of relatively thick cylindrical shells ($R/h \leq 25$), a hardening nonlinear behaviour is present, where the DWCNT analysed in the present paper has thickness ratios $R_1/h = 20.54$ (inner SWCNT) and $R_2/h = 25.68$ (outer SWCNT).

6.4.2. Nonlinear van der Waals interaction forces

In this part, the full expressions of the elastic strain energy (27) and van der Waals interaction energy (42) (i.e. linear and nonlinear terms) are adopted. The goal is to investigate the effect of the nonlinear van der Waals interaction forces on the nonlinear vibrations of DWCNTs.

In Figure 15, the time histories of the dimensionless radial modal coordinate $\tilde{f}_{1,w,1,2}(\tau)$ of the inner SWCNT related with the directly excited mode (1,2) in case of linear and nonlinear van der Waals

interaction forces under the increasing dimensionless modal initial conditions $\tilde{f}_{1,w,1,2}(0)$ of Table 7 are shown. From this Figure it is seen that, by increasing the value of the dimensionless modal initial conditions, the effect of the nonlinear van der Waals interaction forces increases, and a phase shift in time between the modal coordinates corresponding to linear van der Waals interaction energy (blue line) and nonlinear van der Waals interaction energy (red line) close to $\pi/2$ is present at the maximum value of the considered dimensionless modal initial conditions (case F).

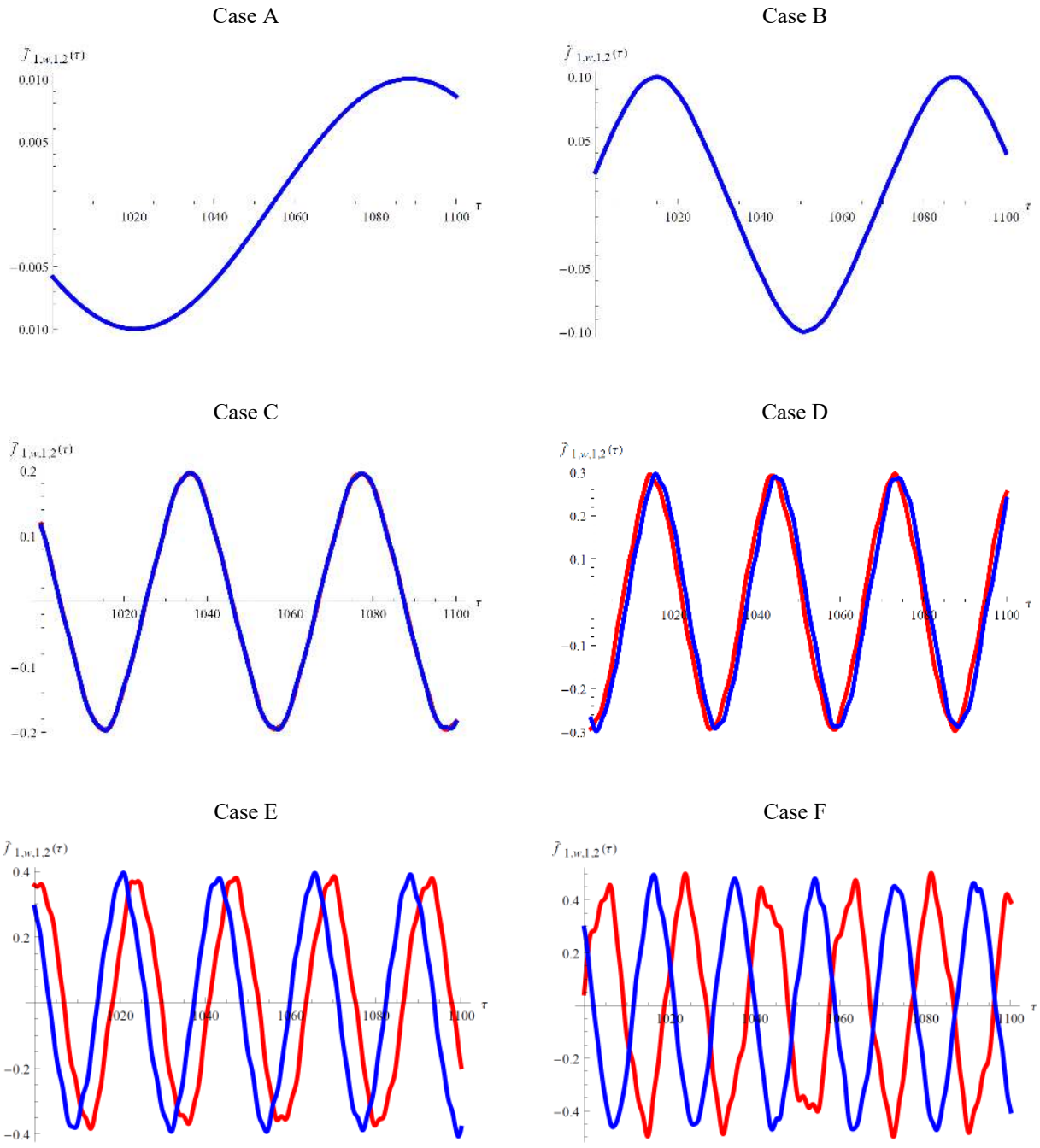

Figure 15. Time histories of the dimensionless modal coordinate $\tilde{f}_{1,w,1,2}(\tau)$ under increasing modal initial conditions of Table 7. —: linear van der Waals interaction energy. —: nonlinear van der Waals interaction energy

Starting from the time histories reported in Figure 15, by adopting the same procedure described in Section 6.4.1, we can obtain the corresponding dimensionless amplitude-frequency responses, in the form of two distinct backbone curves (blue line: linear van der Waals interaction energy, red line: nonlinear van der Waals interaction energy), see Figure 16.

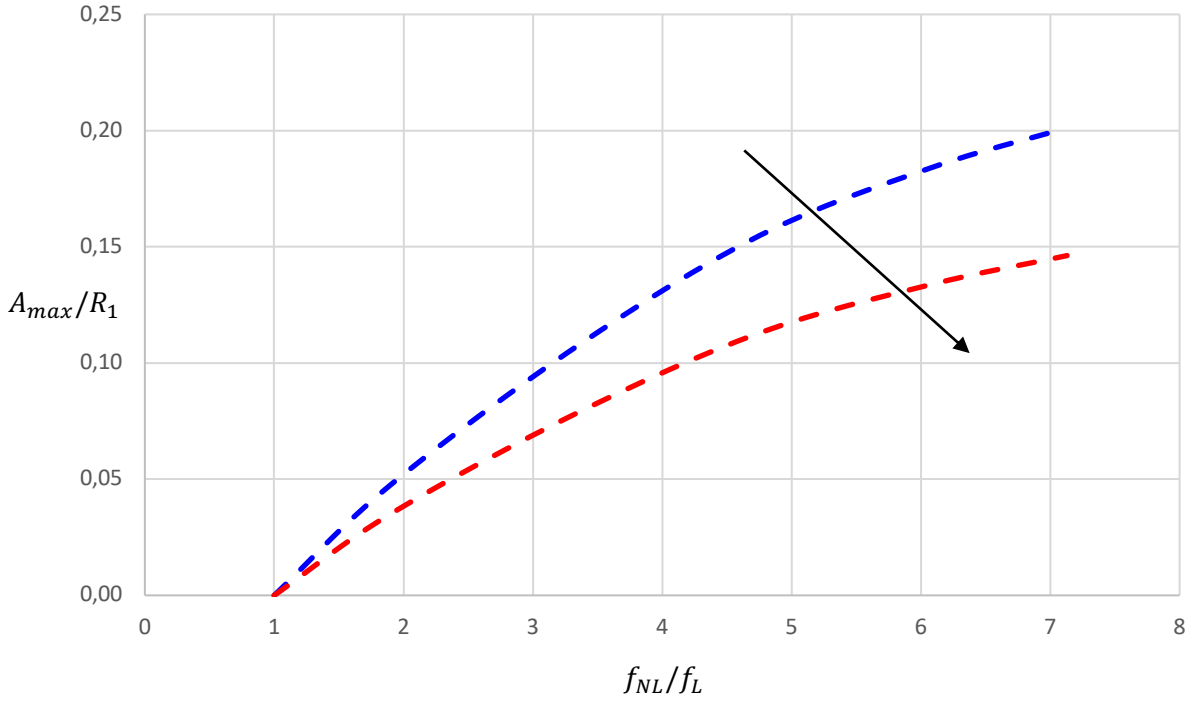

Figure 16. Nonlinear amplitude-frequency curves of the simply supported armchair DWCNT of Table 1. Initially excited mode (1,2) with increasing modal initial conditions of Table 7. —: linear van der Waals interaction energy. —: nonlinear van der Waals interaction energy

From Figure 16 it is observed that the nonlinear behaviour of the considered DWCNT in presence of nonlinear van der Waals interaction forces is more hardening than the one in presence of linear van der Waals interaction forces.

7. Conclusions

In this paper, a novel nonlocal anisotropic elastic shell model to investigate the vibrations of simply supported DWCNTs was proposed. Molecular dynamics simulations were performed to obtain the proper value of nonlocal parameter to be inserted into the constitutive equations of the model. The effect of a nonlinear distribution of van der Waals interaction forces on the nonlinear vibrations of DWCNTs was investigated. The main results are summarised as follows.

- The local model overestimates the natural frequencies compared to MD simulations, where this overestimation increases as the number of longitudinal half-waves m increases, and it is higher for BMs than for CFMs.
- The natural frequencies decrease from the local to the nonlocal model and also as the nonlocal parameter e_0 increases, where this decrease is higher as the number of longitudinal half-waves m increases, and again it is higher for BMs than for CFMs.
- By taking the results of MD simulations as a reference, it is obtained the value of the nonlocal parameter $e_0 = 2$, for which the lowest natural frequency from the nonlocal model is equal to the one from MD simulations, and the estimate of the natural frequencies from the nonlocal model is globally more accurate than that from the local model.
- The amplitude-frequency curve of the considered DWCNT obtained from the nonlocal model under increasing modal initial conditions in presence of a linear distribution of van der Waals interaction forces denotes a hardening nonlinear behaviour.
- In presence of a nonlinear distribution of van der Waals interaction forces (with a third-order nonlinearity), it is found that the nonlinear response of the considered DWCNT is significantly more hardening than that given by the corresponding linear distribution.
- This last result shows that the hardening behaviour of the nonlinear response of the considered DWCNT increases from linear to nonlinear van der Waals interaction force distribution.

Acknowledgements

Matteo Strozzi is grateful to the Department of Sciences and Methods for Engineering, University of Modena and Reggio Emilia (University Research Fund, Year 2021, Call for the equipment financing: Grant FAR_2021_ATTR) for the financial support of this work.

The present work is dedicated to the blessed memory of Professor Leonid I. Manevitch, outstanding educator, respected teacher, admired scholar, who died, after severe illness, on 20 August 2020, at the age of 82. Manevitch followed the research presented in this paper with great attention to the end, dispensing very useful suggestions on mathematical modelling and molecular dynamics simulations. In previously published works, Manevitch investigated nonlinear vibrations of SWCNTs by adopting a local isotropic elastic shell model: the Authors of the present work extended these relevant studies by developing a new nonlocal anisotropic elastic shell model for nonlinear vibrations of DWCNTs.

Author Contributions

Matteo Strozzi Conceptualization; Data curation; Formal analysis; Funding acquisition; Methodology; Software; Visualization; Writing - original draft – review.

Valeri V. Smirnov Data curation; Formal analysis; Software; Validation; Visualization; Writing - original draft.

Francesco Pellicano Conceptualization; Formal analysis; Supervision; Writing - original draft.

Margarita Kovaleva, Conceptualization; Formal analysis; Supervision; Writing - original draft.All Authors have read and agreed to the published version of the manuscript.

Data Availability Statement

All data are available from the Authors.

Conflicts of Interest

The Authors declare no conflict of interest.

References

[1] I. Elishakoff, D. Pentaras, K. Dujat, C. Versaci, G. Muscolino, J. Storch et al. *Carbon Nanotubes and Nanosensors. Vibration, Buckling and Ballistic Impact*. John Wiley & Sons, London, UK, 2012.

[2] S. Bianco. *Carbon Nanotubes – From Research to Applications*. InTech Open, Rijeka, Croatia, 2011.

[3] A. Jorio, G. Dresselhaus, M. Dresselhaus. *Carbon Nanotubes. Advanced Topics in the Synthesis, Structure, Properties and Applications*. Springer-Verlag, Berlin, Germany, 2008.

[4] J.M. Marulanda. *Carbon Nanotubes. Applications on Electron Devices*. InTech Open, Rijeka, Croatia, 2011.

[5] A.M. Rao, E. Richter, S. Bandow, B. Chase, P.C. Eklund, K.A. Williams et al. Diameter-selective Raman scattering from vibrational modes in carbon nanotubes. *Science* 275 (1997) 187-191.

[6] S. Bandow, S. Asaka, Y. Saito et al. Effect of the growth temperature on the diameter distribution and chirality of single-wall carbon nanotubes. *Physical Review Letters* 80 (1998) 3779-3782.

[7] A. Jorio, R. Saito, J.H. Hafner, C.M. Lieber et al. Structural (n,m) determination of isolated single-wall carbon nanotubes by resonant Raman scattering. *Physical Review Letters* 86 (2001) 1118-1121.

[8] S.S. Gupta, F.G. Bosco, R.C. Batra. Breakdown of structural models for vibrations of single-wall zigzag carbon nanotubes. *Journal of Applied Physics* 106 (2009) 063527.

[9] H.C. Cheng, Y.L. Liu, C.H. Wu, W.H. Chen. On radial breathing vibration of carbon nanotubes. *Computational Methods in Applied Mechanical Engineering* 199 (2010) 2820-2827.

[10] S.S. Gupta, F.G. Bosco, R.C. Batra. Wall thickness and elastic moduli of single-walled carbon nanotubes from frequencies of axial, torsional and inextensional modes of vibration. *Computational Material Science* 47 (2010) 1049-1059.

[11] K. Kiani. Vibration behaviour of simply supported inclined single-walled carbon nanotubes using nonlocal Rayleigh beam model. *Applied Mathematical Modelling* 37 (2013) 1836-1850.

[12] P. Pine, Y.E. Yaish, J. Adler. The effect of boundary conditions on the vibrations of armchair, zigzag, and chiral single-walled carbon nanotubes. *Journal of Applied Physics* 110 (2011) 124311.

[13] L. Wang, H. Hu. Flexural wave propagation in single-walled carbon nanotubes. *Physical Review B* 71 (2005) 195412.

[14] K. Kiani, H. Ghaffari, B. Mehri. Application of elastically supported single-walled carbon nanotubes for sensing arbitrarily attached nano-objects. *Current Applied Physics* 13 (2013) 107-120.

[15] I. Elishakoff, D. Pentaras. Fundamental natural frequencies of double-walled carbon nanotubes. *Journal of Sound and Vibration* 322 (2009) 652-664.

[16] B.I. Yakobson, C.J. Brabec, J. Bernholc. Nanomechanics of Carbon Tubes: Instabilities beyond Linear Response. Physical Review Letters 76 (14) (1996) 2511-2514.

[17] J. Peng, J. Wu, K.C. Hwang, J. Song, Y. Huang. Can a single-wall carbon nanotube be modeled as a thin shell? *Journal of the Mechanics and Physics of Solids* 56 (2008) 2213-2224.

[18] N. Silvestre. On the accuracy of shell models for torsional buckling of carbon nanotubes.16 *European Journal of Mechanics A/Solids* 32 (2012) 103-108.

[19] N. Silvestre, C.M. Wang, Y.Y. Zhang, Y. Xiang. Sanders shell model for buckling of single-walled carbon nanotubes with small aspect ratio. *Composite Structures* 93 (2011) 1683-1691.

[20] M. Strozzi, O.V. Gendelman, I. Elishakoff, F. Pellicano F. Applicability and Limitations of Simplified Elastic Shell Theories for Vibration Modelling of Double-Walled Carbon Nanotubes. *C - Journal of Carbon Research* 7(3) 61 (2021) 1-34.

[21] A.W. Leissa. *Vibration of Shells*. Acoustical Society of America, Columbus, OH, USA, 1993.

[22] N. Yamaki. *Elastic Stability of Circular Cylindrical Shells*. Elsevier Printing, Amsterdam, The Netherlands, 1984.

[23] M. Amabili. *Nonlinear Vibrations and Stability of Shells and Plates*. Cambridge University Press, New York, USA, 2008.

[24] A. Muc. Modelling of carbon nanotubes behaviour with the use of a thin shell theory. *Journal of Theoretical and Applied Mechanics* 49(2) (2011) 531-540.

[25] S. Brischetto, O. Polit, E. Carrera. Refined shell model for the linear analysis of isotropic and composite elastic structures. *European Journal of Mechanics A/Solids* 34 (2012) 102-119.

[26] M. Strozzi, L.I. Manevitch, F. Pellicano, V.V. Smirnov, D.S. Shepelev. Low-frequency linear vibrations of single-walled carbon nanotubes: Analytical and numerical models. *Journal of Sound and Vibration* 333 (2014) 2936-2957.

[27] C.Q. Ru. Chirality-dependent mechanical behaviour of carbon nanotubes based on an anisotropic elastic shell model. *Mathematics and Mechanics of Solids* 14 (2009) 88-101.

[28] T. Chang, J. Geng, X. Guo. Prediction of chirality and size-dependent elastic properties of single-walled carbon nanotubes via a molecular mechanics model. *Proceedings of the Royal Society A* 462 (2006) 2523-2540.

[29] T. Chang. A molecular based anisotropic shell model for single-walled carbon nanotubes. *Journal of the Mechanics and Physics of Solids* 58 (2010) 1422-1433.

[30] E. Ghavanloo, S.A. Fazelzadeh. Vibration characteristics of single-walled carbon nanotubes based on an anisotropic elastic shell model. *Applied Mathematical Modelling* 36 (2012) 4988-5000.

[31] A. Favata, P. Podio-Guidugli. A shell theory for chiral single-wall carbon nanotubes. *European Journal of Mechanics A/Solids* 45 (2014) 198-210.

[32] W. Duan, C. Wang, Y. Zhang. Calibration of nonlocal scaling effect parameter for free vibration of carbon nanotubes by molecular dynamics. *Journal of Applied Physics* 101 (2007) 024305.

[33] A.C. Eringen. Linear theory of nonlocal elasticity and dispersion of plane waves. *International Journal of Engineering Science* 10(5) (1972) 425-435.
[34] A.C. Eringen. On differential equations of nonlocal elasticity and solutions of screw dislocation and surface waves. *Journal of Applied Physics* 54(9) (1983) 4703-4710.
[35] Y.G. Hu, K.M. Liew, Q. Wang, X.Q. He, B.I. Yakobson. Nonlocal shell model for elastic wave propagation in single and double-walled carbon nanotubes. *Journal of the Mechanics and Physics of Solids* 56 (2008) 3475-3485.
[36] R. Ansari, H. Rouhi, S. Sahmani. Calibration of the analytical nonlocal shell model for vibrations of double-walled carbon nanotubes with arbitrary boundary conditions using molecular dynamics. *International Journal of Mechanical Sciences* 53 (2011) 786-792.
[37] R. Ansari, S. Ajori, B. Arash. Vibrations of single and double-walled carbon nanotubes with layerwise boundary conditions: A molecular dynamics study. *Current Applied Physics* 12 (2012) 707-711.
[38] S.A. Fazelzadeh, E. Ghavanloo. Nonlocal anisotropic elastic shell model for vibrations of single-walled carbon nanotubes with arbitrary chirality. *Composite Structures* 94 (2012) 1016-1022.
[39] C.Q. Ru. Axially compressed buckling of a double-walled carbon nanotube embedded in an elastic medium. *Journal of the Mechanics and Physics of Solids* 49 (2001) 1265-1279.
[40] X.Q. He, M. Eisenberger, K.M. Liew. The effect of van der Waals interaction modelling on the vibration characteristics of multi-walled carbon nanotubes. *Journal of Applied Physics* 100 (2006) 124317(12).
[41] X.Q. He, S. Kitipornchai, K.M. Liew. Buckling analysis of multi-walled carbon nanotubes: a continuum model accounting for van der Waals interaction. *Journal of Mechanics and Physics of Solids* 53 (2005) 303-326.
[42] X.Q. He, S. Kitipornchai, C.M. Wang, K.M. Liew. Modelling of van der Waals force for infinitesimal deformation of multi-walled carbon nanotubes treated as circular cylindrical shells. *International Journal of Solids and Structures* 42 (2005) 6032-6047.
[43] K. Avramov. Nonlinear vibrations characteristics of single-walled carbon nanotubes by nonlocal elastic shell model. *International Journal of Non-Linear Mechanics* 107 (2018) 149-160.
[44] B. Fang, Y. Zhen, C. Zhang, Y. Tang. Nonlinear vibration analysis of double-walled carbon nanotubes based on nonlocal elasticity theory. *Applied Mathematic Modelling* 37 (2013) 1096-1107.
[45] K.Y Xu, X.N. Guo, C.Q. Ru. Vibration of a double-walled carbon nanotube aroused by nonlinear intertube van der Waals forces. *Journal of Applied Physics* 99 (2006) 064303.

[46] X.Q. He, S. Kitipornchai, C.M. Wang, Y. Xiang, Q. Zhou. A Nonlinear Van Der Waals Force Model for Multiwalled Carbon Nanotubes Modeled by a Nested System of Cylindrical Shells. *Journal of Applied Mechanics* 77 (2010) 061006(6).

[47] L.L. Ke, Y. Xiang, J. Yang, S. Kitipornchai. Nonlinear free vibration of embedded double-walled carbon nanotubes based on nonlocal Timoshenko beam theory. *Computational Materials Science* 47 (2009) 409-417.

[48] E. Cigeroglu, H. Samandari. Nonlinear free vibrations of curved double-walled carbon nanotubes using differential quadrature method. *Physica E* 64 (2014) 95-105.

[49] M. Strozzi, F. Pellicano. Nonlinear vibrations of functionally graded cylindrical shells. *Thin-Walled Structures* 67 (2013) 63-77.

[50] F. Pellicano, M. Amabili, M.P. Païdoussis. Effect of the geometry on the non-linear vibration of circular cylindrical shells. *International Journal of Non-Linear Mechanics* 37 (2002) 1181-1198.

[51] M. Strozzi, V.V. Smirnov, L.I. Manevitch, M. Milani, F. Pellicano. Nonlinear vibrations and energy exchange of single-walled carbon nanotubes. Circumferential flexural modes. *Journal of Sound and Vibration* 381 (2016) 156-178.

[52] M. Strozzi, V.V. Smirnov, L.I. Manevitch, F. Pellicano. Nonlinear vibrations and energy exchange of single-walled carbon nanotubes. Radial breathing modes. *Composite Structures* 184 (2018) 613-632.

[53] M. Strozzi, F. Pellicano. Nonlinear Resonance Interaction between Conjugate Circumferential Flexural Modes in Single-Walled Carbon Nanotubes. *Shock and Vibration* Volume 2019, Article ID 3241698, 33 pages.

[54] F. Rizzetto, E. Jansen, M. Strozzi, F. Pellicano. Nonlinear dynamic stability of cylindrical shells under pulsating axial loading via Finite Element analysis using numerical time integration. *Thin-Walled Structures* 143 (2019) 106213(16).

[55] M. Strozzi, V. Smirnov, L.I. Manevitch, F. Pellicano. Nonlinear normal modes, resonances and energy exchange in single-walled carbon nanotubes. *International Journal of Non-Linear Mechanics* 120 (2020) 103398(19).